Pedro Filipe dos Santos Anjos

Licenciado em Ciências da Engenharia Biomédica

Development of a fundus camera for analysis of photoreceptor directionality in the healthy retina

Dissertação para obtenção do Grau de Mestre em Engenharia Biomédica

Orientador: Brian Vohnsen, Senior Lecturer, University College Dublin, School of Physics

Co-orientador: Pedro Vieira, Professor Auxiliar, FCT-UNL

FACULDADE DE CIÊNCIAS E TECNOLOGIA
UNIVERSIDADE NOVA DE LISBOA

Março, 2015

Development of a fundus camera for analysis of photoreceptor directionality in the healthy retina

This project was developed at University College Dublin within the Advanced Optical Imaging Group.

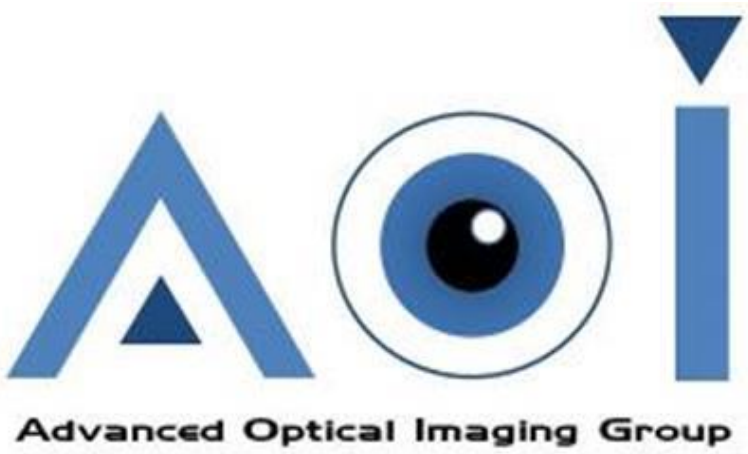

Dedico esta dissertação aos meus avós: Elisabeth Santos, Camilo Luiz dos Santos, Maria José dos Anjos e Carlos Batista dos Anjos.

Por tudo o que me ensinaram e por serem uma fonte de inspiração.

Acknowledgements

I would like to express my appreciation and gratitude to my supervisor Brian Vohnsen for accepting me into his research group, providing me with an amazing opportunity and experience, and for his guidance throughout the project. I would also like to thank PhD student Denise Valente for her support and for the valuable advice at certain key moments. I offer a very special thanks to Salihah Qaysi, just starting her PhD, the person without who the completion of this project would not have been possible. Thank you for your availability and contagious perseverance. Finally, I would like to thank the rest of the Advanced Optical Imaging group: PhD student Rebecca McQuaid, Doctor Atikur Jewel and Doctor Jia Jun Li, for their support and companionship.

I would also like to express my immense gratitude towards my family, for the continuous sacrifices they took on my behalf and for their support, making the conclusion of my Masters studies possible.

Abstract

The Stiles-Crawford effect (SCE) is the well-known phenomenon in which the brightness of light perceived by the human eye depends upon its entrance point in the pupil. This physiological characteristic is due to the directional sensitivity of the cone photoreceptors in the retina and it displays an approximately Gaussian dependency which is altered in a number of pathologies. Retinal imaging, a widely spread clinical practice, may be used to evaluate the SCE and thus serve as diagnostic tool. Nonetheless, its use for such a purpose is still underdeveloped and far from the clinical reality.

In this project a fundus camera was built and used to assess the cone photoreceptor directionality by reflective imaging of the retina in healthy individuals. The physical and physiological implications of its development are addressed in detail in the text: the optical properties of the human eye, illumination issues, acquiring a retinal image formed by the eye, among others. A full description of the developmental process that led to the final measuring method and results is also given.

The developed setup was successfully used to obtain high quality images of the eye fundus and in particular the parafoveal cone photoreceptors. The SCE was successfully observed and characterized. Even though considerable improvements could be done to the measurement method, the project showed the feasibility of using retinal imaging to evaluate the SCE thus motivating its usage in a clinical environment.

Keywords: Eye, Stiles-Crawford Effect, Cone Photoreceptors, Retinal Imaging

Resumo

O efeito de Stiles-Crawford (ESC) é um fenómeno bem conhecido no qual o brilho da luz percepcionado pelo olho humano depende do ponto de entrada da mesma na pupila. Esta característica fisiológica deve-se à sensibilidade direccional dos fotorreceptores na retina, nomeadamente os cones, e apresenta uma dependência aproximadamente Gaussiana que se encontra alterada numa série de patologias. A imagiologia da retina, uma prática clínica comum, pode ser usada para avaliar o ESC e portanto servir como ferramenta de diagnóstico. No entanto, o seu uso para este fim encontra-se ainda sub-desenvolvido e distante da realidade clínica.

Neste projecto, uma câmara de fundo ocular foi criada e usada para aferir a direcionalidade dos cones na retina de indivíduos saudáveis por imagiologia de reflexão. As implicaçoes físicas e fisiológicas do seu desenvolvimento são abordadas em detalhe no texto: as propriedades ópticas do olho humano, questões de iluminação, adquirir uma imagem da retina formada pelo olho, entre outras. Uma descrição completa do processo de desenvolvimento que levou ao método de medição e resultados finais é também feita.

O sistema desenvolvido foi usado com sucesso para obter imagens de alta qualidade do fundo ocular e em particular dos cones na parafóvea. O ESC foi observado e caracterizado com sucesso. Apesar do facto de que melhorias consideráveis pudessem ser feitas ao método de medição, o projecto mostrou a viabilidade do uso de imagiologia da retina para avaliar o ESC e assim motivar o seu uso em ambiente clínico.

Palavras-chave: Olho, Efeito de Stiles-Crawford, Cones, Imagiologia da Retina

Table of Contents

Table of Figures

Table of Tables

1. Introduction

The human eye exhibits directional sensitivity, in which light rays entering the pupil near its centre appear much brighter than those entering closer to the rim of the pupil, this means that the perception of brightness in the eye does not increase linearly with pupil aperture. The effect has been known since 1933 and was named after its discoverers (W. S. Stiles and B. H. Crawford) as the Stiles-Crawford effect (SCE) [1]. Figure 1.1 illustrates the phenomenom.

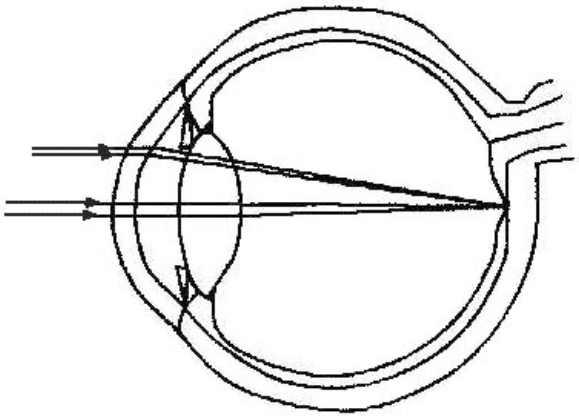

Figure 1.1 Schematic representation of the eye and two bundles of rays entering the eye: one at the center of the pupil and another at its rim. The latter is perceived as less bright [2].

This effect has long been attributed to the photoreceptors in the retina, especially the cones [3]. Cone photoreceptors display waveguide properties, which have come to play a significant role in the explanation of the effect [4]. These optical-fibre like elements, display a high order of parallel orientation towards the centre of the pupil and possess an angle of acceptance which limits the entrance of light to a relatively narrow angle, reducing the amount of obliquely incident light that is absorbed by the photopigments.

The SCE is therefore regarded as a valuable feature of the eye to assess photoreceptor orientation in the retina, which was shown to be disturbed in clinical conditions such as retinitis pigmentosa, central serous choroidopathy, gyrate atrophy, fibrous scars, trauma and age-related macular changes [5].

Nonetheless, its clinical application has seen very limited use, due mainly to the time-consuming psychophysical methods that have been the standard procedures since the discovery of the phenomenon. In such methods, subjects are required to match the brightness of a beam impinging the eye on a distance from the pupil centre, to that of a beam entering the pupil at its centre. Such methods require great concentration and co-operation from the subject, limiting greatly its widespread clinical use [5].

Faster and more practical techniques are therefore demanded. One possible candidate to solve the presented limitations is the manifestation of the related phenomenon of light reflected from the retina. Just like photoreceptors accept light coming from the centre of the

pupil more efficiently, they also reflect it more intensely towards the centre of the pupil [6]; this is called the optical Stiles-Crawford effect (OSCE).

By taking advantage of this optical effect, several techniques have been developed in the last few years; such techniques form what is now termed as fundus reflectometry. Among these methods one may highlight a few: scanning laser ophthalmoscopy [7], imaging spectography [8], optical coherence tomography [9] and retinal photography. The last of these makes use of a fundus camera, which in essence is an ophthalmoscope that redirects the observation light to the film or electronic sensor of a camera.

In this project (developed within the Advanced Optical Imaging Group of the School of Physics, University College Dublin) an in-house built fundus camera is developed and optimized for a minimal impact of aberrations at different angles and wavelengths of illumination of the retina, with the purpose of exploring its directionality on the group members, who will serve as test subjects.

2. Theoretical Background

The eye is the image forming device of the human body. It conveys a comprehensive visual perception of the outer world. Information from exterior objects comes in the form of millions of light rays (or photons) with no particular direction or orientation, the eye gathers those rays through its aperture, the pupil, and bends them with resort to strong lenses, the cornea and crystalline lens, focusing a previously disorganized bundle in one single point on the image sensing layer of the eye, the retina.

The retina is a neuronal tissue layer that covers the posterior wall of the eye, the fundus. It is formed of several intricate intra-layers, one of which is light sensitive, just like the film or electronic sensor of a camera. This layer is formed by tube like photoreceptors which are neurons very generically made up of an inner and an outer segment. Light enters the photoreceptors on the inner segment and is directed towards the outer segment, where it interacts with the photopigments initiating the phototransduction process.

Two types of photoreceptors may be distinguished: cones and rods. Their names come from their outer segments shape, but their differences apart from shape are responsible respectively for: daylight or photopic vision and low light or scotopic vision.

2.1 The Stiles-Crawford Effect

The directional sensitivity of the eye, or SCE, was shown to be retinal in origin [3]. The peak of this sensitivity to light entering the pupil is typically located at approximately 0.2 mm superior and 0.5 mm nasal to its centre (d_{max}) [10] and is traditionally measured in terms of:

$$\eta(d,\lambda) = \frac{amount\ of\ light\ entering\ at\ the\ center\ of\ the\ pupil\ (d=0)}{amount\ of\ light\ entering\ at\ a\ distance\ d \neq 0\ that\ produces\ the\ same\ stimulus}$$

With a Gaussian fit of the form:

$$\eta(r) = \eta_{max} 10^{p(\lambda)(r-r_{\max})^2}$$

Or a parabola fit by taking its logarithm and normalizing:

$$\log(\eta(r)) = \log(\eta_{max}) - p(\lambda)(r-r_{\max})^2$$

$$\frac{\log(\eta(r))}{\log(\eta_{max})} = -p(\lambda)(r-r_{\max})^2$$

Where p, the width of the parabola, is a measure of the directional sensitivity (larger p values correspond to narrower parabolas and greater directional sensitivity) and on average equals 0.05 mm^{-2}; r is the distance to the centre of the pupil.

A representation of the parabola fit is shown in figure 2.1:

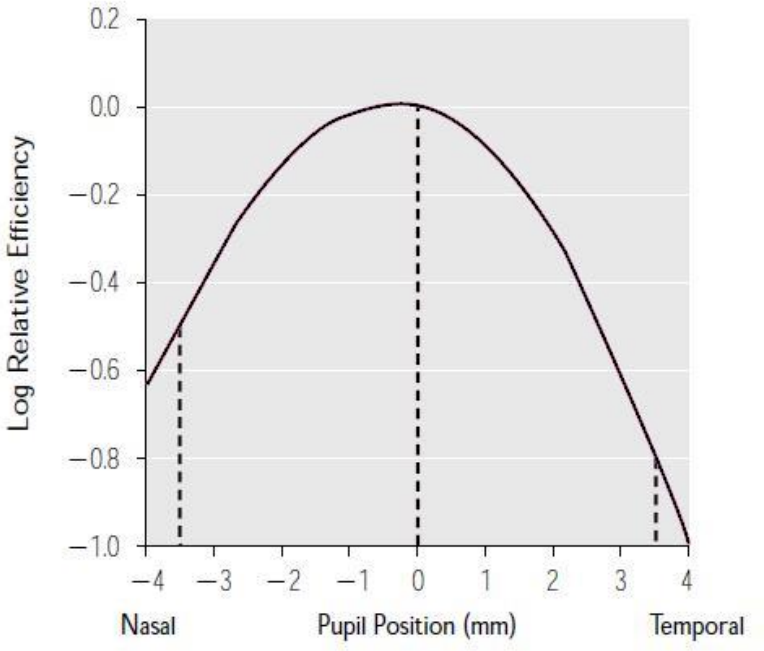

Figure 2.1 The Stiles-Crawford effect in terms of the log relative efficiency of light as a function of pupil position. The dashed lines indicate the center of the pupil and two equidistant points to it. Adapted from [10].

Despite the wide utilization of this representation, it is actually not the most accurate model. The representation based on the Gaussian fit is also widely accepted and shown to provide a more faithful description of the effect [11], especially for pupil locations greater than ±3 mm.

For the Gaussian model the p parameter may be expressed in terms of the half-width at half-height (HWHH) of the Gaussian using the following equation [12]:

$$HWHH = (0.3/p)^{0.5}$$

The directional sensitivity of the eye depends on several parameters, among which luminance and wavelength. When light conditions enable photopic vision, the directional sensitivity remains fairly constant, but when luminous conditions are dim and scotopic/rod vision begins to be predominant, it is greatly reduced. This fact excludes the refractive elements of the eye as the origin of directional sensitivity, suggesting that it must be retinal and manifest itself mainly in cones [3].

The dependence of this phenomenon on wavelength is also highly pronounced [13], being greatest at the extremes of the visible spectrum and least at medium values, between 500 and 600 nm. This feature of the SCE along with the knowledge that the cytoplasm of photoreceptors has a higher index of refraction than the membrane [14], suggest that photoreceptors work as waveguides, or optical fibres, pointing to the centre of the pupil. This also implies an angular acceptance of light by the photoreceptors, which is congruent with the SCE. This is at the present time the basis of the most well established theories to explain the directional sensitivity of the human eye.

2.2 The Waveguide Theory

A waveguide is a structure which confines light by means of total internal reflection, allowing its almost lossless propagation across distances. One such example are optical fibres. To allow for total internal reflection, optical fibres are made up of a core with a high refractive index and a cladding of lower refractive index. Light propagates in the core by being reflected at the cladding at an angle greater than the critical angle required for total internal reflection.

The most widely accepted theories to explain the directional sensitivity of the eye, model the cone photoreceptors as microscopical optical fibres made up of a larger inner segment connected to a thinner outer segment by a tapering region, the ellipsoid [4]. In such model, the cytoplasm of the photoreceptor is regarded as the core and the cell membrane and extracellular fluid as the cladding. Figure 2.2 represents this model:

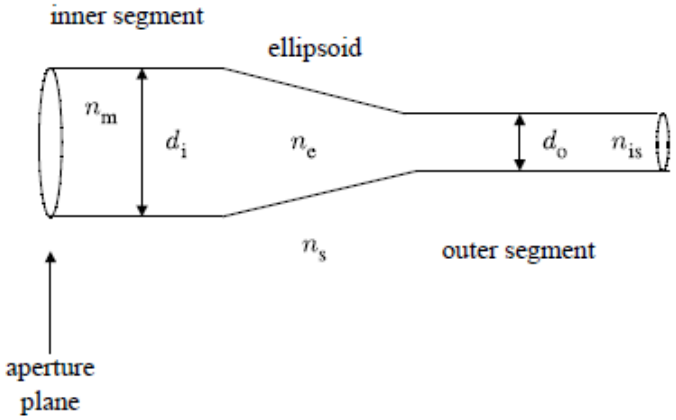

Figure 2.2 Model of a cone photoreceptor used in waveguide theory computations [4]. The diameters d_i and d_o, and the lengths of both segments are obtained from anatomical measurements. The refractive indices n_m, n_s and n_{is} are estimates from mammalian biological preparations.

In the described model, cones are considered as perfect cylindrical structures (apart from the tapering region) with smooth surfaces, which accept light only from one transverse aperture. In addition, all tissue involved is considered to be homogeneous and isotropic.

Since the wavelength of light is in the order of magnitude of the cone aperture, light entering the cone suffers diffraction, originating an ever changing distribution of light propagation angles. Geometrical ray tracing optics is therefore inadequate. Nonetheless, patterns of light distribution that stay constant across the waveguide length are observed, this patterns are characterized by standing waves produced by light bouncing off of the membrane walls that constructively and destructively interfere in this confined region of space [15]. These standing wave patterns are the optical counterpart of the acoustic vibrating string and are likewise called modes.

This wave optics view predicts the existence of several modes in a waveguide, and the number of possible modes and other features of a waveguide are dictated by the important *V* parameter:

$$V = \pi d/\lambda (n_1^2 - n_2^2)^{0.5}$$

Where d is the diameter of the waveguide, λ the wavelength of light, and n_1 and n_2 are the indices of refraction of the core and cladding respectively.

The energy propagating in a mode exists both inside and outside the photoreceptors. While lower order modes possess more energy inside than outside, higher order modes have a lower percentage of their energy within the photoreceptors. Of this energy, only the one contained within the interior of the photoreceptors will be able to interact with the photopigments. Since higher order modes are more efficiently excited by greater angles of incidence, as these angles increase less energy from the trapped light will be interacting with the photopigments and contributing to the brightness sensation.

Although the described approach seems to provide a satisfactory explanation to the phenomenon, one must bear in mind that those are rather simplistic abstract models that make a series of compromises, yielding a formulation that is quite far from the real biological situation [16]. As a consequence, no definitive model of the SCE has yet been established.

The V parameter of the waveguide model is the main factor contributing to the wavelength dependence of the SCE, i.e. the SCE parameter p. An additional effect related to the wavelength of light is the shift in perceived hue and saturation of a monochromatic beam of light when it enters the pupil towards its rim. Such observation has been named chromatic SCE or SCE of the second kind (SCE-2).

2.3 The SCE of the Second Kind

As observed by W. S. Stiles in 1937, light entering the eye pupil at a distance from its centre will not only seem less bright, it will also change its apparent color [17].

This phenomenon is characterized by a shift of the hue of short and long wavelengths to the hue of longer wavelengths, whereas medium wavelengths shift their perceived hue to those of shorter wavelengths. Moreover, supersaturation occurs in wavelengths greater than about 515 nm and desaturation in wavelengths between 515 and 480 nm [18]. The magnitude of the shift and the point at which it reverses direction differ greatly between individuals.

The perception of a specific color hue by the human eye is obtained from the relative amount of photopigment stimuli between each cone type (short, medium and long wavelength cones) [19]. Therefore, changes in relative photopigment photon absorption numbers must be the basis for the phenomenon.

Two main factors are thought to influence these numbers: the changing of spectral sensitivity of cones with changing incident angle and differences in morphology and refractive indices between the three cone types [20]. As previously stated, when light enters a photoreceptor at greater angles, higher order modes of propagation are excited. These higher order modes have less energy inside of the photoreceptor, thus producing less photopigment photon absorptions and as a consequence a narrowing of the spectral sensitivity of the photopigment takes place. This process is called self-screening. On the other hand, if the three cone types exhibit systematic differences between each other, then its waveguiding properties

will differ as well, resulting in different numbers of photon absorptions between cone types for varying incident angles.

2.4 Biological Function

The SCE can be regarded as a reduction of the effective diameter of the pupil – an apodization –, a gradual reduction in opposition to a sharp cutoff provided by the iris. This effect has the consequence of reducing off-axis rays entering the eye, thus reducing the amount of aberrated rays contributing to form an image. Although this effect is thought to give little contribution to image quality in eyes with normal focusing ability, it was shown to provide greater image quality in accommodation lag situations or in ametropic eyes [21].

The several elements of the eye, from the cornea to the fundus itself, are known to produce scatter phenomena. These events contribute to the glare we see around luminous points of light. By being able to select light that comes from the centre of the pupil, the retina filters out to some extent the scattered photons that deteriorate image quality.

A further advantage of this pupil apodization comes from the fact that it manifests mainly in cone photoreceptors. Since rods require large pupil diameters to maximally absorb larger amounts of light whereas cones provide more acute images with non-aberrated, non-scattered light, the SCE provides a clever means to allow optimum rod and cone simultaneous functioning in medium light conditions (mesoscopic vision), by reducing the pupil effective diameter for cones while maintaining the real pupil dimensions for rods [12].

An additional possible purpose of waveguiding in the retina, is that it might be advantageous to have the photopigments packed in a smaller region of space, this way photopigment production and maintenance may be more cost efficient while simultaneously allowing for an equivalent photon absorption of a larger area.

2.5 The Optical SCE

Most of the light reaching the retina is absorbed either by the photopigments, contributing to forming an image, or by other elements in the fundus such as the retinal pigment epithelium (RPE) or the choroid. Nonetheless, a very small percentage of the light reaching the retina is always reflected back to the pupil [6].

The reflectivity of the retina is explained by two main processes: backscattering and photoreceptor waveguiding [22]. The first happens as a result of those photons that reach the extracellular space in between photoreceptors and are scattered back, resulting in a relatively uniform distribution of reflected light at the pupil plane with no considerable directional component which produces a constant background in the reflectance profile. The second, is due to the recapture of light that is reflected at the RPE after fully traversing the photoreceptors without being absorbed by the photopigments, being posteriorly redirected towards the pupil centre and producing a reflectance profile similar to that of the SCE.

This last feature of the reflectance of the retina, clearly reflects the directionality of the eye and constitutes a measure of the SCE, it is therefore called the optical Stiles-Crawford effect, in contrast to the psychophysical SCE. It also suggests that better measurements may be carried

by bleaching the photopigments with a relatively strong light source, thus reducing the amount of absorptions of the incident beam by the photopigments.

The intensity distribution of the optical SCE is usually fitted to a Gaussian, like the psychophysical SCE, with the additional sum of a constant background component, the scattering component:

$$I = B + I_{max} 10^{-p(\lambda)(r-r_{\max})^2}$$

Where B is the constant background.

Figure 2.3 shows a graph of a measurement and respective fit:

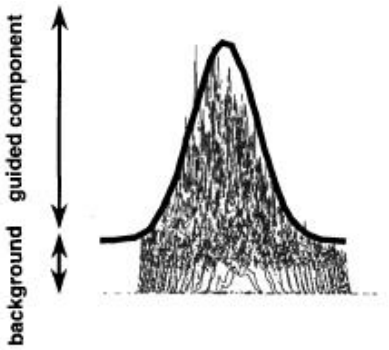

Figure 2.3 Measured values for the optical Stiles-Crawford effect fitted to a Gaussian curve [22].

The speckle effect present in the data is thought to be due to the coherent interference between wavelets with different phases, produced by neighbor photoreceptors which possess slight differences in their lengths.

Another important feature of the optical SCE is the value of the p parameter, which is always at least twofold that of the psychophysical SCE. A possible explanation comes from the fact that a redistribution of the energy inside the cones takes place when light is recaptured after being reflected at the RPE [23]. This recaptured light, travelling backwards inside the cones, is thought to excite less efficiently higher order modes. Just like light entering the cones at larger angles excites more efficiently these modes, light coming out from these modes is also emitted with wider angles. Thus, a reduced propagation of light in higher order modes, results in a narrower emission of light from cones.

The optical SCE is the motivational principle for the development and use of a wide range of reflectometric systems that gauge the SCE by means of a fast optical measurement. The fundus camera, with its wide range of applications in retinal diagnosis, may as well be regarded as a tool for such measurements.

2.6 The Fundus Camera

As the name indicates, a fundus camera is a device designed with the purpose of acquiring images of the eye fundus and recording them in some way. In order to accomplish this, light must be projected on the fundus and regathered after bouncing off of its surface, just like in any photograph. Such endeavor has however a few particularities in the case of the fundus of the eye: light must enter and leave the "place" where the subject of interest is, by the same relatively small "hole", the pupil; the eye has its own refractive system which bends light entering and leaving the "hole"; finally, the subject of interest, the retina, reflects very little light when compared with the other optical elements present in the process, either those from the camera system or from the eye itself [24].

A very simple way to photograph the eye fundus is to take a portrait photograph with a normal camera using a flash, the famous red eye effect is no more than the choroid reflection from the eye fundus. But when trying to do the same at a closer, more useful distance, all we get is a black round hole. This happens because the flash is imaged in a certain region of the fundus, instead of illuminating the whole fundus (due to the refraction of the eye), while what the observer sees through the patient's pupil is the image of another region of the patient's fundus [25]. Figure 2.4 illustrates the situation.

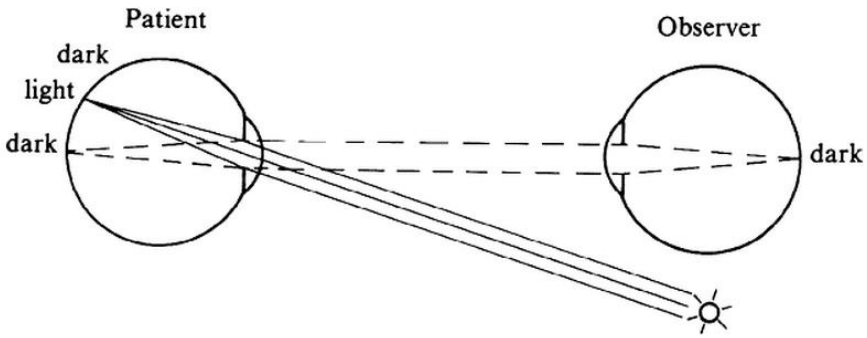

Figure 2.4 The region that the observer is able to see stays dark, while the light from the illuminated region is reflected towards the source [25].

In order to solve this issue, the light source must be made collinear or near collinear with the observer, this way the observer will be seeing the illuminated area of the patient's eye. On the other hand, the illumination beam and the observation (imaging) beam must be separated on the cornea surfaces and on the crystalline lens anterior surface, in order to prevent light of the illumination beam from being reflected at those surfaces and interfere with the imaging beam [26].

These two apparent incompatible requirements may be met by the use of an annulus mirror and a convex lens, or objective lens. The two elements are placed such that the annulus mirror lies in the pupil conjugate plane, in which the patient's pupil is magnified. The light source is then shaped into an annulus by a diaphragm, imaged by another set of lens at the annulus mirror and reimaged at the pupil plane [24]. Light will thus enter the eye through the periphery of the pupil and exit at its centre, as shown in figure 2.5, this way both illumination and observation beams will be separated, while maintaining collinearity.

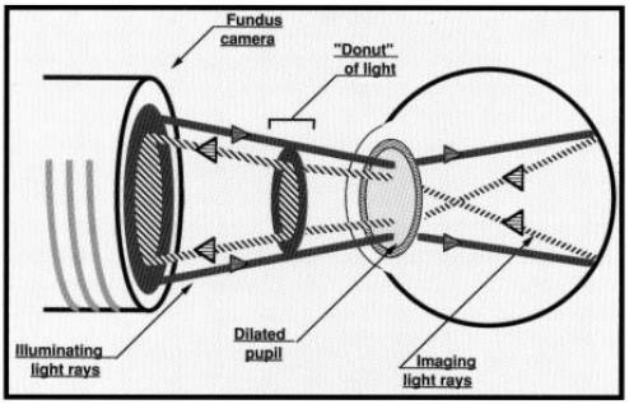

Figure 2.5 Diagram showing light entering the eye at the periphery of the pupil and leaving at its center [28].

Therefore, the inner circle of the annulus delimits the observation region at the pupil plane, the area from which the observation beam comes out with the visual information of the fundus. This region is also called the total entrance pupil (TEP), because it encloses the total area of each individual entrance pupil, each of which is determined by the eccentricity angle of the fundus region under study and the parameters of the lens system: refractive indices, thicknesses and curvatures [27].

The annulus inner circle also determines how much of the peripheral zone of the fundus is illuminated: with smaller diameters, larger eccentric angles become illuminated. However, by reducing this diameter we are concomitantly reducing the total entrance pupil. The size of the eye pupil on the other hand, dictates how much of the central region of the fundus gets to be illuminated: with larger pupil diameters, smaller eccentric angles become illuminated. Figure 2.6 clarifies these issues.

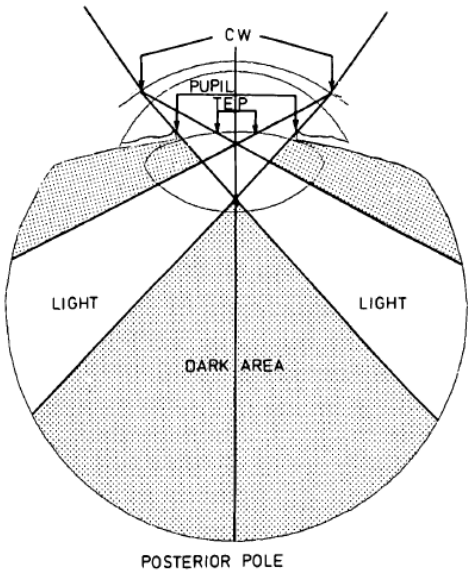

Figure 2.6 Diagram of the illumination of the fundus. If the pupil is enlarged, a larger area of the posterior pole will be illuminated. On the other hand, by enlarging the TEP, less peripheral fundus regions will be illuminated. CW stands for corneal window, the inner circle of the annulus at the corneal plane. [27]

After leaving the eye, the observation beam reenters the objective lens which forms an aerial image of the retina at its focal plane, behind the annulus mirror, with the imaging beam

passing through its hole. If the fundus camera allows for wide angle imaging, a lens or set of lenses named field lens may follow the objective lens to help bring the aerial image to focus in a linear plane by choice of appropriate individual entrance pupils. Finally, a zoom lens which the observer operates focuses on the aerial image of the retina, creating an image on the film of the camera. An additional astigmatism correction lens is also commonly present. Figure 2.7 shows a diagram of such a system.

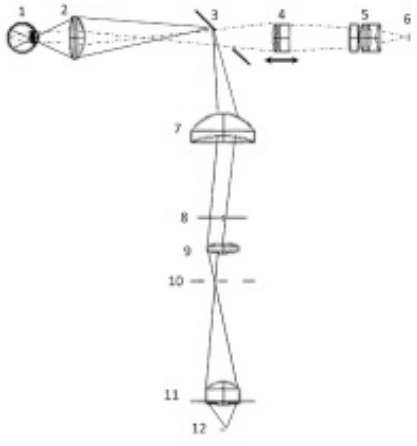

Figure 2.7 Simplified diagram of the optics of a fundus camera. The camera film lies in point 6. 12 is the light source, 10 the diaphragm, 3 the annulus mirror, 2 the objective lens, 4 the focusing reticle and 5 the zoom lens. [24]

To allow the camera operator to focus the retinal image on the camera film, a mirror and a prism are used [28]. The mirror stands in front of the film making a 45º angle with it, deviating the image upwards in a 90º angle. The prism is placed above the mirror such that the image is once again redirected in a 90º angle towards the observer eye. The base of the prism is placed precisely at the same distance from the mirror and making the same angle with it, as the film does. The operator should therefore focus the image of the retina in the base of the prism. In order to prevent the operator's eye from accommodating on an image formed in a plane which is not in the base of the prism, etched black lines are printed in a glass which lies in this plan. This lines form the focusing reticle. The operator must focus his eyes on this reticle before focusing the retinal image with the zoom lens. When both the focusing reticle and the retinal image are seen in focus, the operator presses the camera shutter and the mirror is raised allowing the image to fall on the film of the camera, like in an SLR camera. Figure 2.8 exemplifies the process.

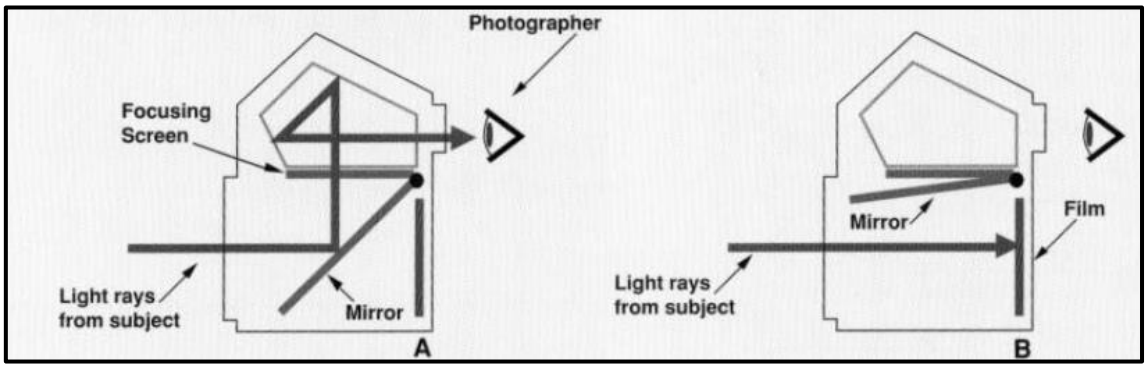

Figure 2.8 Illustration of the mirror and prism system used in the camera. [28]

3. State of the art

A variety of techniques have been employed by several authors to measure the directionality of the photoreceptors in the human retina. Gao et al. [9] explored the directionality of different layers in the retina through the use of optical coherence tomography (OCT), Gorrand & Delori [32] developed a reflectometric technique that measures photoreceptor alignment by gauging the reflected intensity at the pupil, Zagers et al. [8] measured foveal spectral reflectance and cone directionality using an imaging spectrograph.

Although part of the content of the previous section may already be regarded as state of the art, in this section three specific works with major relevance to the project are briefly analyzed. The first of those, borrows a technique from astronomy to obtain high-resolution images with a fundus camera; the other two were developed within the same research group as this project was developed: a scanning laser ophthalmoscope technique and a numerical analysis approach.

3.1 Adaptive optics and retinal imaging

J. Liang, D. R. Williams, and D. T. Miller have successfully used adaptive optics to obtain high-resolution images of the in-vivo human retina to an extent that was only possible to date in ex-vivo samples [29]. By using this technology, A. Roorda and D. R. Williams have studied the optical fibre properties of individual human cones [30].

The concept behind adaptive optics is to correct the natural aberrations of the human eye allowing for higher resolution images of the retina. The human eye is not a perfect focusing device, even with the most acute of visions it presents a host of higher order aberrations that blur vision and reduce the quality of images of the retina. When in bright light conditions, the eye can afford to reduce pupil size allowing a reduction of these aberrations; nonetheless, a smaller pupil size also results in less spatial resolution due to diffraction effects. Thus, by reducing aberrations of the eye while keeping large pupil sizes, high resolution images of the retina may be obtained and vision acuity may be further enhanced.

The adaptive optics module integrated in the fundus camera developed by Roorda and Williams, is made up of two phases: the wave-front sensing and the wave-front compensation. Figure 3.1 illustrates the configuration of these elements within the camera:

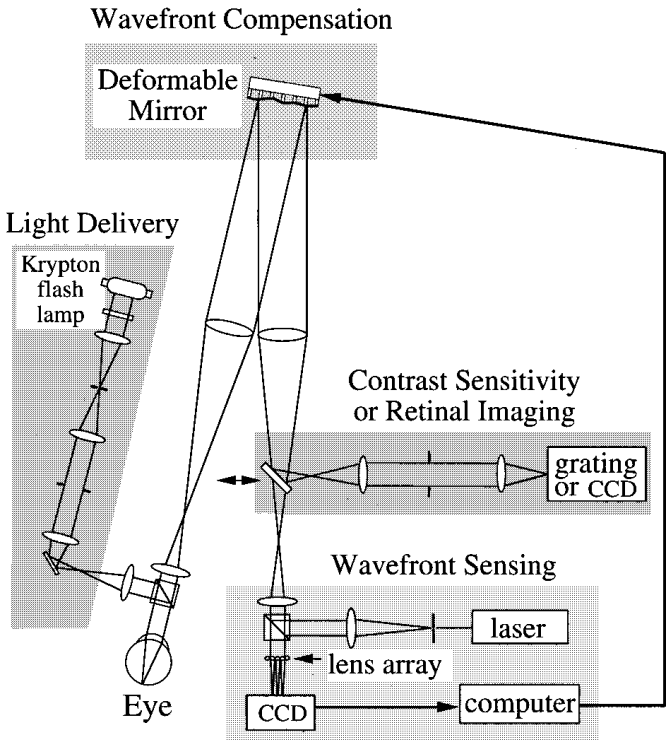

Figure 3.1 Diagram of the optical system used. [29]

The first phase comprises a Hartmann–Shack wave-front sensor, which consists of an array of 217 small lenses (lenslets) conjugate to the pupil plane, each lenslet with a diameter of 0.5 mm, a centre-to-centre distance of 0.4 mm and a focal length of 97 mm. Behind the lenslet array lies a scientific-grade CCD with 512×512 pixels. A laser beam is focused by the eye onto the retina, which in turn reflects some of the light towards the pupil; this light is then gathered by the lenslet array with each lenslet forming an image of the wave-front on the CCD that lies behind. The displacement of each image gives the local wave-front slope, which is then used to construct the total wave-front slope using a least squares fit.

The second phase of the wave-front correction module comprises one deformable mirror with 37 actuators, each actuator 7 mm apart and producing a local deformation of ±2 μm in 4096 steps (12 bits). The mirror lies on the conjugate plane of the pupil, which is magnified 6.25 times on the mirror plane, translating the actuator spacing to 1.12 mm in the pupil plane. Light coming from the eye is reflected by the mirror in its flat configuration towards the sensor, which is also in the conjugate plane of the mirror, the sensor and computer measure the wave-front aberration and compute the required mirror deformation. This information is then sent to the mirror actuators completing a closed-loop circuit. After corrected by the proper mirror deformation, a high resolution image of the retina is captured. Figure 3.2 shows a superimposed diagram of both wave-front sensor and deformable mirror.

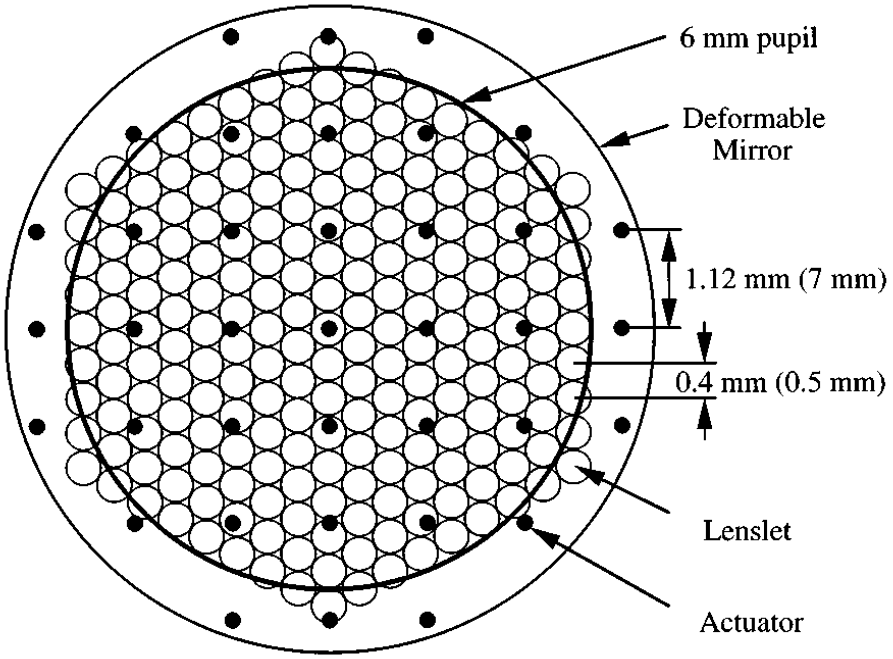

Figure 3.2 Representation of the wave-front sensor and mirror actuators superimposed at the pupil plane. The values in parentheses correspond to real the physical spacing. [29]

A. Roorda and D. R. Williams were able to show that the amount of disarray in human cones is locally correlated and that it is not enough to account for the spread of the total angular tuning function of the retina.

In this experiment, the same patch of cones 1º nasal from the fovea was imaged with seven different illumination angles. A pair of images was randomly taken for each incidence angle. After seven pairs of images were taken, the wave-front aberrations were corrected and the random process was repeated again until 20 images of each incidence angle were obtained. From those 20 images, the ten 10 best were chosen, added together and aligned with sub-pixel accuracy.

The locations of a series of adjacent cones within a 3×3 pixel region was identified and the average reflected intensity of each cone was measured and fitted using a least-mean square method. Figure 3.3 shows the location of each identified cone and respective orientation and orientation magnitude in relation to the cone group considered. The amount of disarray and how it is locally correlated can be easily observed.

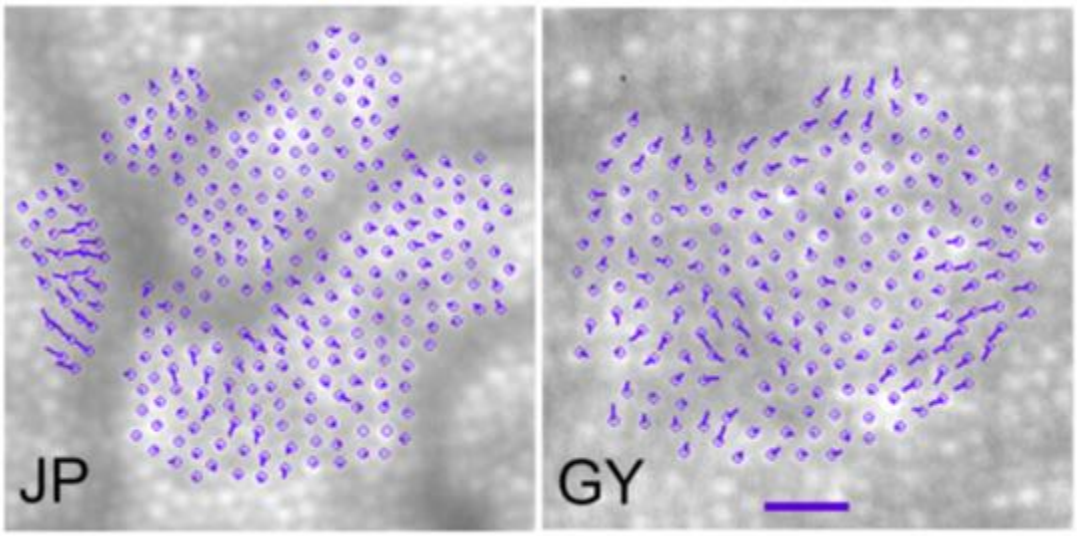

Figure 3.3 Cone directionality plots, superimposed with the retinal images of the 2 subjects. JP and GY are the acronyms of the test subjects. [30]

Although cone disarray is observable, the measured disarray accounts for about only 5% of the total angular tuning spread, which concludes that measurements of the tuning function of a group of cones, independently of its size, should be almost identical to the effective tuning function of a single cone.

3.2 Ultra-small spot size scanning laser ophthalmoscopy

D. Rativa and B. Vohnsen developed a scanning laser ophthalmoscope (SLO), capable of resolving single cones with resort to beam spot sizes of ultra-small dimensions [31] and showed that individual cone directionality is more pronounced than the average directionality of an ensemble of cones [7].

In order to resolve single cones in the retina with an SLO, beam spot sizes must be of the order of magnitude of individual cone diameters and incident along their respective axis, optimizing radiative transfer and light-coupling efficiency to the propagation modes of cones. A small confocal pinhole is also essential to avoid unwanted scattered light.

Smaller beam sizes may be accomplished by the use of smaller wavelengths, larger pupil sizes (with increased aberrations) or resorting to annular beams. In this work the last option was explored. By applying a circular stop to the beam centre, an annulus beam was produced. Adding this stop to the beam reduces the full width at half maximum (FWHM) of the point spread function (PSF) of the beam on the retina, as shown in figure 3.4, allowing for smaller beam spot sizes and consequently enhancing mode coupling in smaller cones.

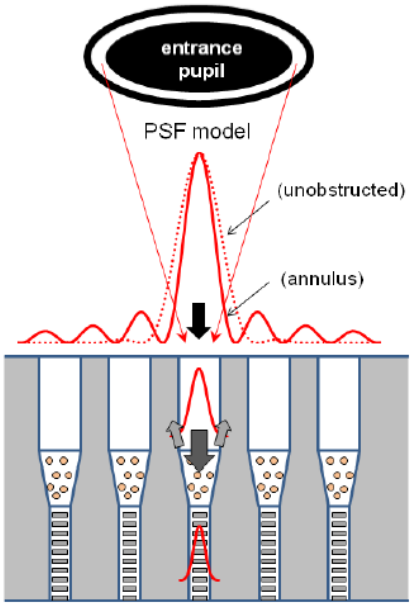

Figure 3.4 PSF comparison between the unobstructed and annulus beams. The annulus beam provides a narrower PSF, comparable to the photoreceptor diameter. [31]

The images are acquired at a rate of 47 fps by two scanners (one vertical and another horizontal) located at conjugated planes of the pupil. The eyes of the subjects were fixated at angles of 2.5º, 5º, 10º, 15º and 20º using a distant LED as a fixation target, and the directionality values obtained by acquiring the intensity values in steps of 0.35 mm along the pupil scan.

Due to the considerably small size of the cones at the fovea, individual cone directionality values cannot be reliably obtained for this region; therefore, average values were obtained for regions from 0º to 1.5º. For eccentricities larger than 2º, the assessment of individual directionalities becomes available. Directionality values ranging from 0.08 to 0.12 mm^{-2} were found at an eccentricity of 2.5º, increasing approximately threefold at eccentricities around 20º. However, when averaged across a small group of cones (boxes in Figure 3.5), the directionality obtained was around 0.14 mm^{-2}, and if averaged across the whole image, the values fall to approximately 0.12 mm^{-2} at any of the measured eccentricities.

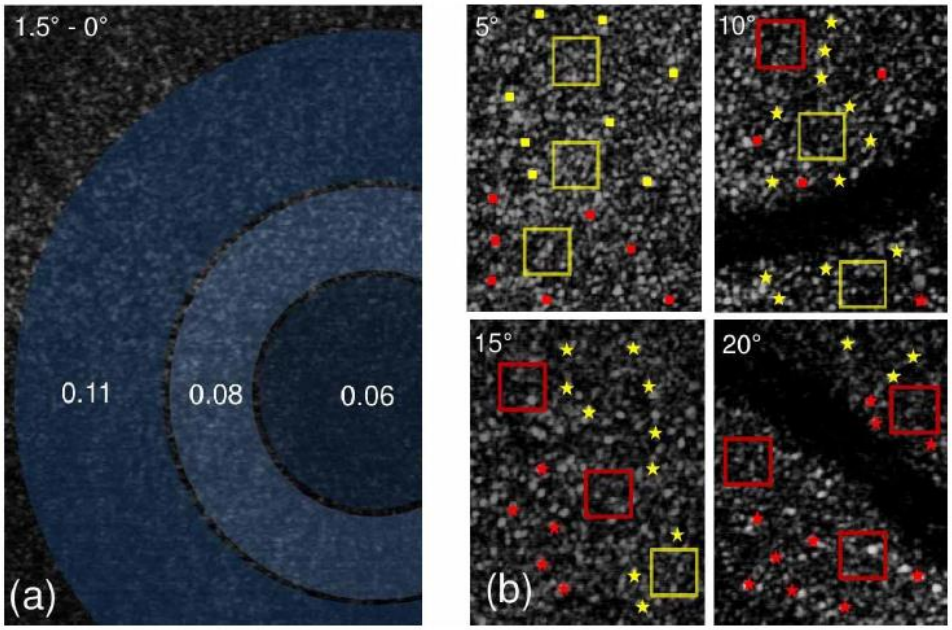

Figure 3.5 Retinal images and directionality values obtained for one of the subjects. a) Average directionalities for circular regions at 0.65º, 1º and 1.5º from the fovea. b) Individual directionalities for four different eccentricities – yellow box and yellow square: p = 0.10 - 0.15 mm^{-2}; red box and red square: p = 0.15 - 0.20 mm^{-2}; yellow star: p = 0.20 - 0.30 mm^{-2}; red star: p > 0.30 mm^{-2}. [7]

3.3 A layered scattering model of outer-segment photoreceptor pigments

B. Vohnsen developed a model of the photoreceptor outer-segments based on stacked layers of photoreceptor pigments to study the electromagnetic interactions of pigments with light, showing the versatility of such models to study several properties of the retina, including its directionality [33].

OCT techniques have revealed that different directionality parameters may be found in different photoreceptor pigment cells along the photoreceptors axis, even without a directional filtering from waveguiding [9]. Such findings incite a more thorough study of the photopigment cell layers in photoreceptors and especially the electromagnetic interactions they undergo with light.

Although a variety of techniques allow photoreceptor visualization, this is made possible mainly due to the reflection of light on the high index mitochondria present in the inner-to-outer segments junction of the photoreceptors, therefore, no technique developed to date is actually able to image photopigment cells and give insight into its interactions with light.

In this work, two different models of the photoreceptors are presented, one macroscopic and another microscopic, those are illustrated in figure 3.6. Both models are based on a stack of photopigment layers where waveguiding is excluded allowing for diffraction beyond the

photoreceptor walls, and optical reciprocity is assumed, which implies that the radiative properties of the model are proportional to its light gathering properties.

The macroscopic model is based on the fact that photopigment molecular density is very high and it may therefore be regarded as constant across each layer for far-field measurements. The photoreceptor is thus modeled has a stacked array of equidistant, parallel discs that are actually circular apertures, allowing for simpler calculations based on diffraction and paraxial light propagation.

The microscopic model takes into consideration single photopigment cells and the nanometric space they occupy. In this model, each molecule is considered as a light-induced point-dipole antenna that coherently emits and receives electromagnetic radiation. A full treatment of the electromagnetic interaction is therefore obtained, allowing for calculations in the vicinity of the photoreceptors and offering a greater insight into the electromagnetic role of individual photopigments in the process of vision.

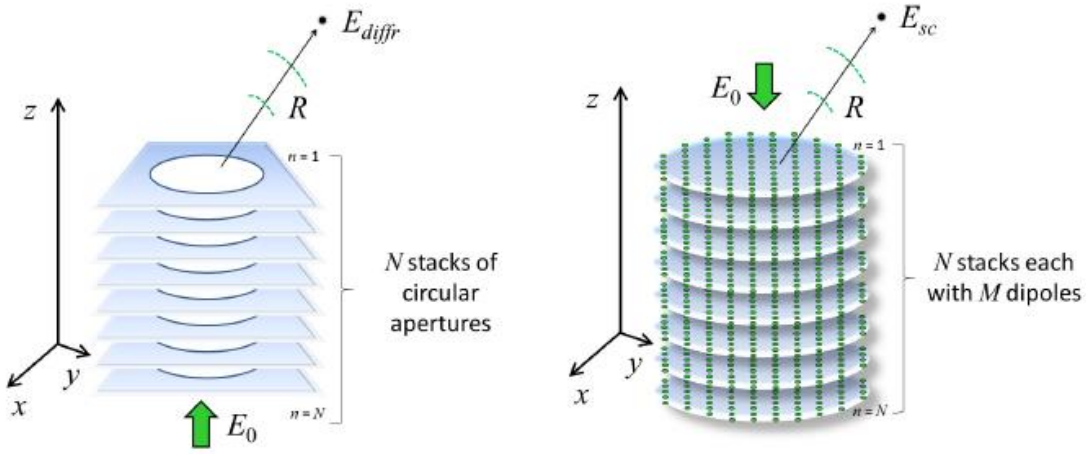

Figure 3.6 Macroscopic and microscopic outer-segment models. [33]

Both models yield similar results at the pupil plane and show a good concordance with experimental data for photoreceptor directionality, revealing that the developed method may have important applications in the modelling of relevant questions regarding light-photoreceptor interactions, even though waveguiding is excluded. The obtained Stiles-Crawford functions further reveal a dependence on outer-segment diameter, length and on the wavelength of light.

4. Work plan

This project builds up from the work of two Master's students who developed a fundus camera with the purpose of imaging the vessels in the human retina.

In a first phase, the previously conceived setup was reassembled and modified with the aim of reducing the exposed area of the retina, obtaining a greater magnification and allowing the visualization of the cone mosaic in the parafovea with reasonable resolution.

Once an acceptable setup has been achieved, preliminary tests of the system were conducted in order to obtain optimum illumination and focus conditions with a minimal impact of aberrations and system reflections. High quality retinal images were obtained at this point.

Directionality measurements were then undertaken in group-member eyes for verification of the system and demonstration of the Stiles-Crawford effect.

5. Camera Design Considerations

Some considerations must be taken into account when designing a fundus camera, some of those have already been introduced in a previous section of this dissertation in the context of a commercial fundus camera. In this section, such considerations are extended and analyzed in greater detail in the context of the present problem. These concerns became relevant as the project unfolded.

5.1 Optical Properties of the Eye

The human eye, already introduced in chapters 1 and 2, may be regarded as an intricate optical system comprising several optical elements: lenses, apertures, a light sensitive device and its own propagation media which forms a structure to hold everything in place.

Just like in any optical system, a myriad of different variables and characteristics of these optical elements influence the passage of light through the system and consequently its performance. This performance affects not only the image formation of the outer world inside of the eye, but also the opposite process of forming an image of its interior that is captured by an external imaging device.

5.1.1 Refractive elements

Two main elements form the refractive machinery of the eye: the cornea and the crystalline lens. When imaging the retina, one must take into consideration the fact that the object under study is not within direct reach, it lies instead behind these refractive elements that change the way light reaches it and is reflected from it. The total refractive power of the unaccommodated eye sums to approximately 60 D which translates to a focal distance of approximately 16.7 mm [34].

The cornea constitutes two thirds of the refracting power of the eye. It is an aspheric surface, flattening away from the vertex, made up of several layers with an average refractive index of 1.376 and a refractive power of approximately 42.2 D. The stroma, the main layer, constitutes 90% of the cornea and is composed of collagen lamellae disposed in regular arrays providing transparency and structure. The outer layer of the cornea, the tear film, forms an oily and aqueous coating that moistens and smoothens the rough surface of the cornea, maintaining its transparency; due to its considerably fast drying, frequent blinking is essential to maintain high image quality.

The large difference in refractive indices between the air and the cornea is responsible for the refraction of light entering the eye, but as a consequence, some of the light is also reflected from the cornea, approximately 3% of the incoming light. This poses a major difficulty when imaging the retina, due to the production of considerable veiling glare, as the retina itself only reflects about 0.1% of the incident light. This disadvantage may be overcome by asking the test subject to look slightly away from the illumination spot to separate the reflected light from the image or by taking advantage of the birefringence of the eye.

The second lens of the eye, the crystalline lens or simply lens, is responsible for the rest of the refracting work of the eye. Unlike the cornea, the lens is able to change its refracting power in order to focus on close objects. For the emmetropic eye, this power change ranges from 19 D, in an eye focused for infinity, to 30 D, if the eye focuses in an object 10 cm away from the cornea. This process is called accommodation, and it holds a major influence in the formation of an image of the retina outside the eye: the distance at which the eye is focusing is also the distance where an image of the retina will be formed.

The effect of the eye lenses may nonetheless be changed in some individuals. When this occurs, an eye is said to be ametropic or to have refractive error. This condition influences retinal image formation depending on the kind of refractive error: if an eye is myopic, either the fundus is elongated or the refractive power of the eye is abnormally increased, as a result a retinal image will always be formed closer to the eye instead of at infinity; on the other hand, if the eye is hypermetropic either its fundus is shortened or the refractive power of the eye is abnormally reduced and it will be required that the test subject accommodates in order to produce an image of the retina at infinity; finally, when an eye exhibits astigmatism, the refractive power of the eye lenses is different depending on its axis, forming a retinal image which displays a gradual blurring along one of the axis. Refractive errors may be corrected by the use of lenses that compensate the abnormal power of the eye, and they may be inserted in the experimental setup or used by the test subject as spectacles.

Another property of the cornea and lens that may be used advantageously in retinal imaging is the fact that the propagation of light inside them is dependent on the polarization, this property takes by the name of birefringence and it is due to the regular structures of these tissues. Thus, linearly polarized light entering the eye will exhibit a change in polarization when leaving it. This property may be exploited to reduce corneal reflections through the use of simple polarizer filters; this approach is explored in greater detail later in the text.

5.1.2 Aperture

The aperture stop of the eye is formed by the iris, it lies between the cornea and the crystalline lens; both the image of its aperture as formed by the cornea and the aperture itself are commonly called the eye pupil, nonetheless, the former is the one usually measured. As in other optical systems, the eye pupil controls the amount of light entering the eye: in response to high intensity levels the pupil constricts to a minimum of less than 2 mm in diameter and extends up to 8 mm in low light levels [34].

Just like for any other aperture, light passing through the eye pupil is diffracted, this means that the ability to resolve two points in an image is affected by the size of the pupil. Reducing the size of the pupil smears out the image of a single point, resulting in poorer resolution; on the other hand, increased pupil sizes reduce the effects of diffraction, relaying a less smeared out image of each point in the object resulting in improved resolution [35].

Large pupil sizes should ideally therefore always be desirable; however, this is not the case: as pupil size increases so does the allowed entrance angle of light into the eye and aberrations start to settle in. Image formation inside and outside the eye takes place due to the refraction of light by the lenses of the eye, this refraction is ruled by Snell's Law which has a sinusoidal

dependence, as the angle of the entrance of light into the eye increases the higher orders of the sine expansion in Snell's Law start to have an effect and not all the light coming from a single point of the object will converge onto the same point in the image space, resulting in a blurred image. This is what is called optical aberration [36].

Diffraction and aberrations are a major source of image deterioration in retinal imaging. Figure 5.1 shows the effect of diffraction on the Airy disc in comparison with the effect of aberrations. The optimal diameter range that produces the best balance between diffraction and aberration effects is estimated between 2.5 and 3 mm, which occurs in bright light conditions [34].

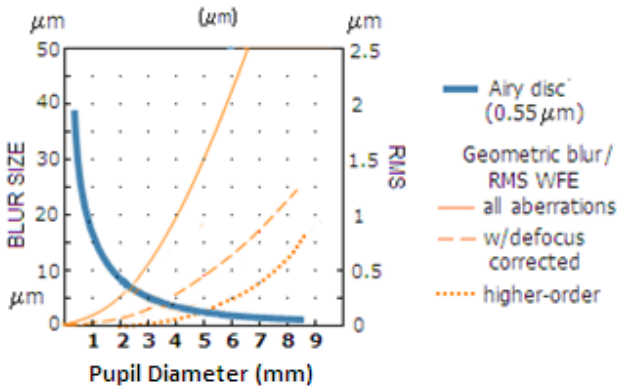

Figure 5.1 Diffraction vs aberrations effects in the eye [37].

Pupil diameter also influences the depth-of-field of the formed image. When an image is formed it shows only a plane of the object space in perfect focus, points of the object space in other planes are reproduced as defocused circles of confusion, causing blur. The range of distances in the object space which produce circles of confusion smaller than the sensor detecting units is called the depth-of-field. Larger pupil diameters result in faster increases of the circle of confusion with increasing distance from the optimal focus plane, which translates to a narrower depth-of-field; conversely, a smaller pupil diameter produces smaller circles of confusion and therefore greater depth-of-field. When imaging the retina, a small pupil will contribute to have several planes of the retina being in good focus, whereas a larger pupil will produce an image with good focus in fewer planes of the retina.

5.1.3 Sensitive Surface

The sensitive surface of the eye, the retina, has in the present problem the role of the object under study, constituting the object space. Composed of several physiological layers that absorb and reflect light in different ways, the retina exhibits a complex reflective response which depends mainly on the wavelength of light. Generally speaking, shorter wavelengths of light will penetrate less before experiencing reflexion, a reflexion which is also more specular in nature; whereas longer wavelengths of light will tend to go deeper into the layers of the retina and reflect more diffusely [35].

In the overall, the retina has greater reflectance for longer wavelengths, which may be partly explained by the fact that the cornea and lens absorb a considerable amount of the shorter wavelength light and in addition the most reflective layer of the retina, the retinal pigment epithelium, reflects mainly in the longer wavelength light provided that the visual pigments are bleached [34]. Figure 5.2 shows the reflectivity of the retina at different wavelengths as presented by several authors.

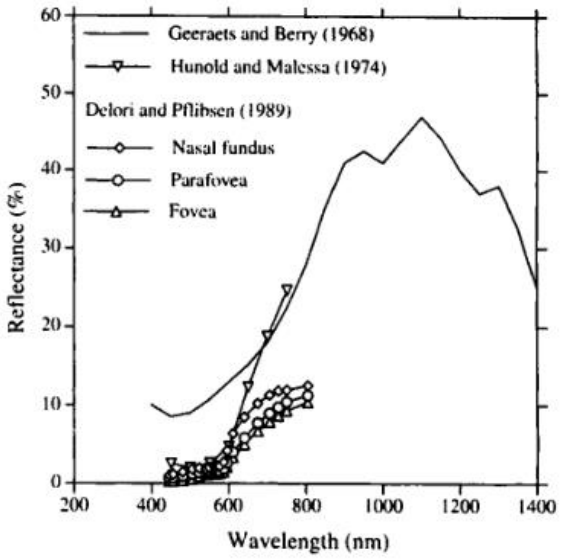

Figure 5.2 Spectral reflectance of the fundus from three different groups of authors [34].

Reflectance around the wavelength of green light is also of particular interest in the present problem since two of the three types of cones have a greater sensitivity to green light (550 nm). Once bleached, those cones will show greater reflectance when using such wavelength of light, allowing for a cone selective reflectance of the fundus [38].

5.2 Eye motion

Eye motion is another major source of image degradation when imaging the retina. While imaging the retina, the subject is asked to keep his/her eye still, however, miniature eye movements are always present, these involuntary movements of the eye are necessary to overcome natural optical defects of the normal human eye and to correct the drifting from the target under fixation [39]. Two possible methods may help reduce the effect of these movements when imaging: devising a complex optical arrangement that counteracts these movements [39] or using very short acquisition times.

5.3 Illumination

When illuminating the retina, it is desirable to keep the illumination elements off axis, so that the retinal image formed in front of the eye may be captured. Nonetheless, the illumination and imaging beams must be made collinear as was already discussed. The illumination beam is therefore produced out of the line of sight of the subject and directed towards the eye afterwards. To do so, three different approaches were attempted during the

development of the camera, each differing on the optical element used to deviate the light towards the eye: a beam splitter, a mirror and a very thin optical fibre.

Other illumination concerns include the size, illuminance and uniformity of the illuminated region of the retina, the focusing of the eye, the existence of corneal reflections and the fact that it should be possible to choose a specific entrance point within the pupil to allow the required measurements of the Stiles-Crawford apodization curve.

5.3.1 Maxwellian Illumination

These aspects may be addressed by the use of Maxwellian view, an eye illumination method in which the light source is imaged onto the pupil plane, as shown in figure 5.3 [35].

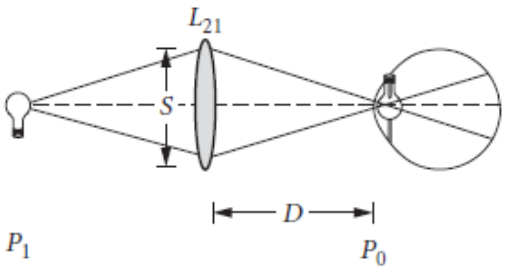

Figure 5.3 Representation of a simple Maxwellian view system [35].

By using a positive lens, a small image of the source may be produced in the pupil plane, which translates to a rather minute illumination spot on the pupil, ideal to undertake directionality measures by moving the source sideways and changing its entrance point across the pupil. In addition, corneal reflections are reduced and illumination conditions are independent of the eye's pupil size.

The fact that the source is imaged on the pupil plane and then spreads out uniformly, also allows the production of a bright and uniform illumination field on the retinal plane whose size, illuminance and focus can be independently controlled.

5.3.2 Illuminated Region

The size of the illuminated region of the retina may be specified in two ways: its area or its angular subtense at the pupil. The knowledge of the area is necessary to understand the relation between the size of the eye, focal lengths and the intensity of light used. On the other hand, angular subtense is independent of the optical properties of the eye, depending solely in external measurable parameters; such characteristic makes it the most widely used [35].

In Maxwellian view, the illuminated area, S_r, is determined by the areal magnification provided by the system eye/lens, scaled by an aperture stop placed at the retinal conjugal plane:

$$S_r = (f_e/f_1)^2 \times S_A$$

Where f_e is the focal of the eye, $f_1$is the focal length of the Maxwellian lens and S_A is the area of the aperture stop.

The angular subtense, α, may be computed by considering figure 5.3. The tangent of the half angular tense is equal to the ratio of the radius of the illuminated area and the focal length of the eye. By measuring the diameter of the aperture stop placed at a conjugal plane of the retina (it is impossible to directly measure the radius of the illuminated area of the retina), the angular subtense may be obtained:

$$tan(\alpha/2) = \frac{(d/2)}{f_e}$$

$$\alpha = 2 \times tan^{-1}(d/2f_e)$$

Where d is the diameter of the illuminated area on the retina or the diameter of the aperture stop.

The illuminated region of the retina is therefore mainly determined by aperture stops.

5.3.3 Illuminance

The light available in the system (the luminous flux ϕ) is determined by the area of the source, its luminance, the aperture of the system and the focal length of the lens used [35]:

$$\phi = S_S L_S S_A / {f_1}^2$$

By dividing luminous flux by the illuminated area, the illuminance of the retina is obtained:

$$E_R = \frac{\phi}{S_R} = S_S L_S / {f_e}^2$$

As it can be seen, the illuminance of the retina depends only on the area of the source and its luminance, being independent from the aperture stops. By changing its area, both luminous flux and illuminated area change, canceling each other.

5.3.4 Eye Focus

The Maxwellian view method allows control of the focus of the eye. By placing a target after the light source one focal length away from the lens, at the retinal conjugate plane, the image of the target will be at infinity and a real image is produced at the retina of a non-accommodated emmetropic eye. On the other hand, by placing the target closer to the lens, a virtual image is produced and the subject will be required to accomodate in order to focus on this image. The focus of the eye may thus be changed according to necessity [35].

An alternative illumination method using a very thin optical fibre was briefly explored in this project. This is exposed in greater detail in another point of this dissertation.

5.3.5 Positioning the Subject

The first problem arising when positioning a subject is the fact that his/her head must be still in order to reduce undesired eye motion. Head movements may be suppressed by the use

of a chin rest, a wax impression of the subject's teeth (bite bar) or any other device that may help stabilize the movements of the head. This device should then be attached to a mechanism which allows accurate displacements in order to position the subject's eye [35].

Once the subject's head is stabilized, the centre of the eye pupil must be precisely positioned at the focal point of the source image, in order to establish the viewing system previously described. The first step is to position the eye at the right distance from the Maxwellian lens; to do so, the subject's head is moved sideways at several distances close to the focal point, this will occlude the source image if the eye is in the wrong plane. When the correct plane is achieved, the image of the source will be seen by the subject as uniformly dimming, instead of being occluded on the sides. A second person, or the experimenter, may also help on locating this distance by observing the image of the source on the eye pupil while moving the person's head closer or farther from the lens.

Following this process, the image of the source, or illumination spot, must be centered in the eye pupil. By displacing the head sideways such that the spot becomes occluded by the iris as seen by the subject, first to one side then the other, the horizontal centre of the pupil may be obtained as the centre between these two positions. By repeating the process vertically, the pupil may be centered.

5.4 Acquiring an Image

Once the retina is illuminated, its image will be formed by the lenses of the eye at the infinite outside the eye. One or more lenses are then required to focus this image onto an image sensor. A few concerns regard the development of this part of the system, these are discussed here.

5.4.1 Field of View and Magnification

How much of the image formed outside the eye is captured by the system is determined by the size of the lens following the eye and the distance between both. Figure 5.4 helps understand the concept.

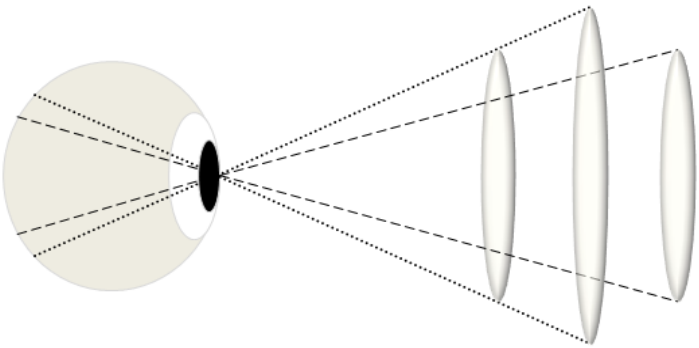

Figure 5.4 Change in the field of view depending on lens distance and diameter.

The farther the lens is from the eye or the smaller its diameter, the smaller the angle of view will be. In order to more accurately quantify the dimension of this angle a similar expression to the angle of the illuminated region may be used:

$$\alpha = 2 \times tan^{-1}(d/2s)$$

Where now d is the diameter of the lens, and s the distance between the pupil and the lens.

An image will be formed at the focal distance of the lens. The magnification of this image may be approximated through the thin lens combination equation [36]:

$$M = \frac{f_1 s_{i2}}{d(s_{o1} - f_1) - s_{o1} f_1}$$

Where f_1 is the focal length of the first lens (counting from the object towards the final image), s_{i2} is the distance from the second lens to the image formed by it, d is the distance between both lenses and s_{o1} the distance from the object to the first lens.

In the present situation the first lens may be considered to be the lenses of the eye, the final image is formed by the second lens at its focal length and the distance from the object to the first lens is the focal length of the eye, therefore:

$$f_1 = f_e \quad ; \quad s_{i2} = f_l \quad ; \quad s_{o1} = f_e$$

The magnification of the system 'eye plus lens' may thus be obtained by the ratio between the focal length of the lens used and the focal length of the eye:

$$M = \frac{f_l}{f_e}$$

Following this lens, a second lens may be desirable to increase magnification, to help changing the plane of focus in the retina or simply to refocus the retinal image enhancing its quality and allowing to view the whole image formed by the first lens.

This second lens will focus on the aerial image formed by the first and produce a new image whose magnification will depend on its distance from the aerial image, s_o [36]:

$$M_2 = \frac{f_2}{s_o - f_2}$$

The total magnification is given by the product of both steps of magnification:

$$M_T = M_1 \times M_2$$

Increasing magnification will also further reduce the field of view. The greater the magnification, the closer the second lens must be to the aerial image and the farther the image is formed; considering the fact that the sensor size stays the same, the field of view will be reduced, as figure 5.5 clarifies.

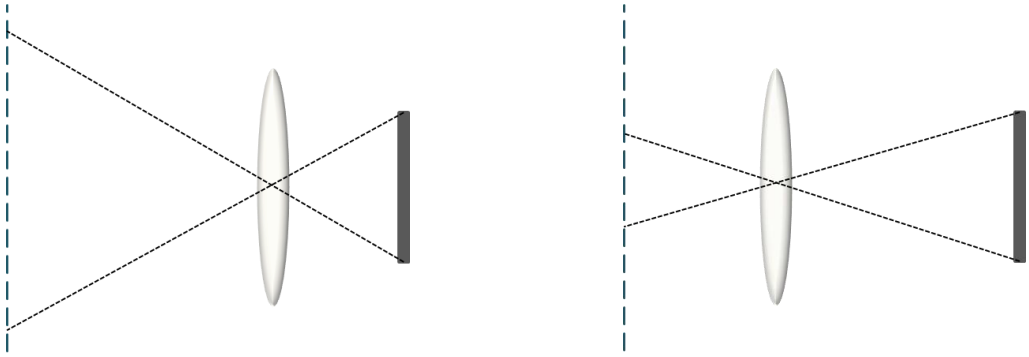

Figure 5.5 Influence of magnification on the field of view. In the first case a smaller magnification is obtained and a greater one in the second case. The vertical dashes represent the aerial image.

If the magnification is small enough so that the whole aerial image stays within the field of view of the second lens plus sensor, then the field of view of the system is given by the field of view of the first lens. This will not only allow to see the whole image formed by the first lens (which otherwise could prove impossible depending on sensor size) but also improve the quality (if the magnification is less than 1) since the same amount of light will be focused in a smaller area.

On the other hand, if the aerial image is not completely captured, then the new field of view must be calculated. Consider figure 5.6.

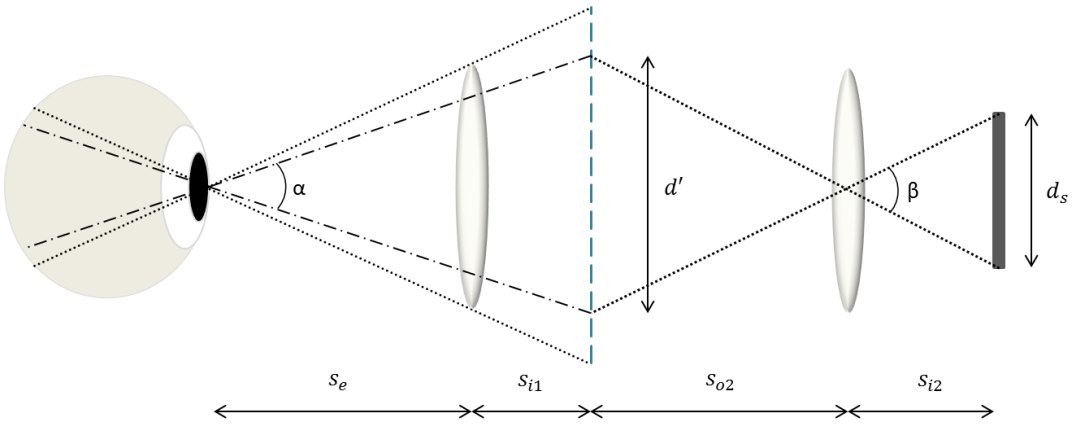

Figure 5.6 Reduced field of view after image magnification.

The angle β may be obtained through an expression identical to angle α with no second lens:

$$\beta = 2 \times tan^{-1}(d_s/2s_{i2})$$

Once angle β is known, d' may be obtained:

$$d' = 2.s_{o2}.\tan(\beta/2)$$

This new diameter d' may now be used to compute the field of view:

$$\alpha = 2 \times tan^{-1}\left(\frac{d'}{2(s_e + s_{i1})}\right)$$

5.4.2 Changing the focusing plane and magnification

The different layers of the retina lie within slightly different distances from the pupil, as a result, these layers are simultaneously imaged by the first lens at slightly different planes. By moving both the sensor and second lens back and forth, the second lens will be focusing on different aerial images, so that different planes of the retina will be focused by the system and different layers will be imaged, while keeping the magnification unchanged. If no second lens is used the same may be accomplished by moving the sensor alone.

If only the sensor is moved (considering two lenses are being used), the magnification will be modified with only a minor change of the plane under focus. This happens because when a lens is close to an object, the magnification will be increased by bringing it closer to the object; however, the displacement of the magnified image will be considerably larger than the displacement of the lens towards the object. This means that by moving the sensor alone away from the second lens for example, a magnified image of an aerial image slightly closer to the second lens will be acquired, and therefore a slightly more superficial layer of the retina will be imaged. Nonetheless, this change in the plane under focus is so small when compared with the increase in magnification, that it may be neglected.

We may in this case more easily obtain the magnification provided by the second lens by measuring the distance between the sensor and the second lens and applying the following expression [36]:

$$M_2 = \frac{s_{i2} - f_2}{f_2}$$

5.5 Shielding

As previously mentioned the amount of light reflected from the retina is extremely small, therefore a sensor with a considerably high sensitivity is required in order to capture the image. This also means that any other source of light other than the retina will add background noise to the final image occluding the real retinal image.

These sources of unwanted or stray light are, in their majority, considerably stronger than the reflection from the retina and originate from the illumination apparatus, reflections from several surfaces in the system, corneal reflections and possible sources which are not part of the system. It is therefore of absolute importance to impede as much as possible this light from reaching the sensor. To accomplish this, low reflectance dark shields may be used to isolate the different parts of the system, especially the imaging components from the illumination apparatus and elements. Metallic components should also be covered by black card and the whole system covered by a soft black material, eliminating light coming from outside into the system.

5.6 Health and Safety

When working with light and real human eyes one must take into consideration the possible hazards to the health of the individuals being submitted to the experiment. These hazards may be divided into two main types depending on the underlying mechanism: thermal and photochemical [35].

Thermal damage to the eye basically means overheating or burning of the tissue due to absorption of light and its conversion to heat. Although it is predominant at longer wavelengths, it takes place over a wide range of the visible and IR spectrum regions, and is mainly dependent on the exposure duration being therefore a rate process with dependence upon the time-temperature absorption history of a volume of tissue as a whole. It also means longer exposure times will require a lower critical temperature to induce damage.

Photochemical damage is the loss of electrons by the molecular constituents of cells due to the absorption of light [40], resulting in the production of reactive radicals and free electrons with harmful consequences for the eye tissue. Unlike the thermal reactions, this kind of reaction is highly dependent on the wavelength of light and displays action spectra in the shorter wavelength and UV regions of the electromagnetic spectrum, which usually have a Gaussian-like shape with a full width at half height of less than 100 nm. An action spectrum is a curve describing the effectiveness of light in causing biological damage photochemically, depending on its wavelength. This process exhibits as well a characteristic reciprocity between the irradiance E $(\mathrm{W/cm^2})$ and exposure duration t (s): $H = E.t$; this value, H, the radiant exposure $(\mathrm{J/cm^2})$ may be used to express the injury threshold.

For the past few decades, the aforementioned hazards to human health have been thoroughly studied and guidelines have been conceived to avoid eye injury during experiments with light. The American National Standards Institute *(ANSI)* provides a set of guidelines that may be used to calculate the maximum permissible retinal irradiance (MPE_r). By using an optical power meter, the irradiance of the illumination spot in the eye may be controlled and maintained under the calculated value. These guidelines and calculations are shown in appendix A.1.

6. Optical Elements and Other Tools

The setup employed for this project was developed on an optical table where all the elements were mounted. In this section a brief description of the materials used throughout its development is given.

Light Source:

The light source used was a *Dolan-Jenner MI-150* optic fibre illuminator with a 150 W tungsten halogen lamp equipped with a knob to adjust intensity. One of two optical fibres was fixed to the output of the illuminator, allowing a more controlled positioning of the light source of the system.

Optical Fibres:

Two different optical fibres were used at different stages of the project. The first, a *Dolan-Jenner Industries* optical fibre had a 1.59 mm diameter fibre bundle and a 68 degrees acceptance cone and was used in the Maxwellian view approach.

A second optical fibre was used experimentally for a short period of time. This was a much thinner fibre, with a 0.4 mm diameter core and a 0.73 mm diameter including the cladding and a buffer. This fibre could be cut according to need, and the cladding and buffer could be removed by burning.

Filters:

Two types of filter used during the project may be distinguished: colour filters and polarizer filters.

The first of those are common coloured filters which allow the passage of light with a wavelength within a bandwidth around one particular value depending on its colour. Two colours were used: red and green.

The second type of filter used is a linear polarizer filter. Such kind of filter selects only one particular direction of polarization of the incoming light, so that its output has a well-defined linear polarization [36].

Iris Diaphragm:

An iris diaphragm is an opaque structure with a controllable aperture at its centre. It is used to stop light and therefore control its amount in a system. Two irises with adjustable diameter between 1 and 36 mm were used at different stages of the project to reduce stray light in the system, to control the size of the illumination spot in the pupil, change the depth of field/focus of the images or reduce optical aberrations.

Lenses:

Two types of converging lenses were used throughout the project: simple biconvex lenses and achromatic doublet lenses, both manufactured by *Thorlabs*. Preference was given to the latter, those allowed for a considerable reduction of spherical and chromatic aberrations and also possess anti-reflective coating for wavelengths between 400 and 700 nm. Biconvex lenses were used only when no achromatic doublet with a specific focal length was available and were not used in the final setup.

All lenses used in the setup were 25.4 mm in diameter. One 12.7 mm diameter lens of 19 mm focal length was used along with a black target or a paper to simulate the eye lenses and the retina.

Beam Splitter:

A beam splitter is a surface that transmits only part of an incident beam and reflects the rest of it [36]. A 50:50 plate beam splitter was used to make the illumination and imaging paths collinear by reflecting 50% of the light from the source towards the eye and still allowing part of the light coming from the retina to reach the image sensor (50%).

Shutter:

An optical shutter is a device used to control the duration of the passage of light into an optical system. The shutter used was the *Thorlabs SH05* with an aperture of 12.7 mm and its respective controller, the *SC10* model from the same company, which allows a minimum exposure time of 10 ms and can be controlled manually, triggering the opening and closing of the shutter by pressing an external button, or externally, using the imaging sensor software or other software.

sCMOS Imaging Sensor:

The imaging sensor used throughout the project was the *Andor Neo 5.5* scientific Complementary Metal-Oxide-Semiconductor (sCMOS) image sensor. It allows high resolution imaging even at extremely low light levels, with rapid frame rates and a wide dynamic range while maintaining low noise levels, making it an ideal choice for scientific applications [41].

The sensor consists of a two-dimensional array of microscopic light sensors, or pixels, installed in a large metallic structure along with the required electronics and cooling system. Each of the microscopic sensors generates electrons through the photoelectric effect depending on the amount of light detected and a dedicated electronic circuitry translates these electrons into a voltage value in each pixel. Each column of pixels has its own amplifier and an analog-to-digital converter. How the voltage is read from the pixels into each column amplifier and then converted into a digital signal depends on the choice of the user between one of two modes: rolling shutter and global shutter modes [42].

The rolling shutter mode consists of a split readout method in which the upper and lower halves of the sensor are read independently. The exposure starts at the central lines of the sensor and proceeds to its periphery. As exposure in each line finishes, the readout step begins, starting at the central lines and sweeping across the sensor one line at a time, until its

top and bottom edges, the process is shown in figure 6.1. This mode is the most advisable for most applications, since it allows for superior frame rates and lower noise levels.

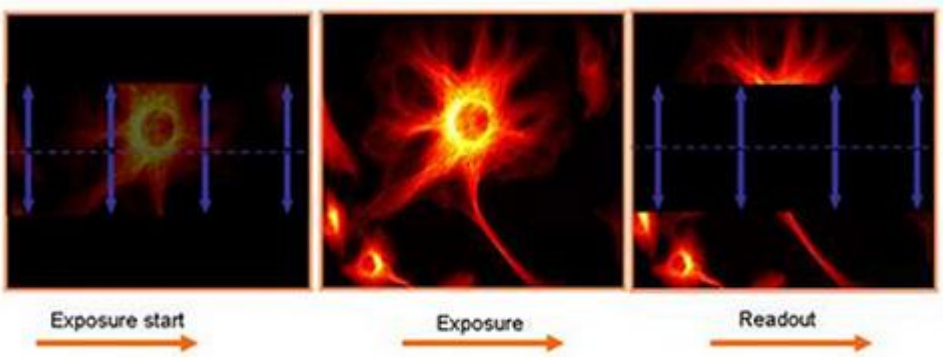

Figure 6.1 Rolling shutter mode exposure sequence. [41]

The downside of rolling shutter mode is the spatial distortion while imaging fast changing scenes, when these changes are faster than the sampling wave across the sensor, plus the difficulty in synchronising the acquisition with external switching devices. To overcome such inconveniences, a global shutter mode is featured in the sensor. In this mode all the pixels in the sensor are exposed at the same time and once exposure finishes all pixels information is readout, amplified and converted to the digital signal, it is therefore also called snapshot mode, figure 6.2 illustrates the process. Due to the simultaneous reading of a greater amount of information and since only one image may be acquired at a time, the RMS reading noise is increased by a factor of 1.41 and the maximum frame rate is halved.

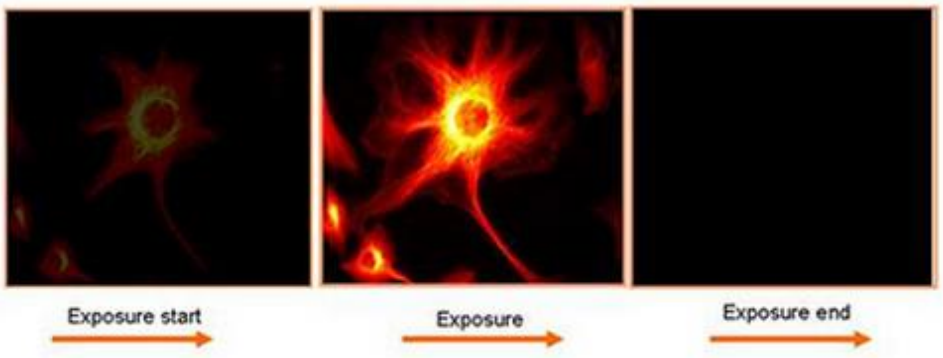

Figure 6.2 Global shutter mode exposure sequence. [41]

Since no fast moving scenes were studied, the rolling shutter mode was the preferred one to undertake the experiments throughout the project.

The technical specifications of the sensor, such as size and number of pixels, are included in appendix A.2.

LED:

An LED was used at several stages of the project to serve as a fixing point for the test subject, in order to maintain a certain region of the retina under the field of view.

Shielding:

The shielding used was low reflectance black card which was cut into several different shapes according to need and put in place using black tape. A large low reflectance black cloak was also used to cover the whole system.

Bite-bar:

A bite-bar was used to hold the subject's head in place. A super hydrophilic impression material from *Dental Product Report* was used to produce an impression of the subject's teeth by asking the subject to bite the heated material bar. Once cooled, the material hardens and preserves an impression of the subject's teeth, which may be used as a bite-bar for stabilization of head movement.

Movable Stages:

Millimetric movable stages are ideal for precise millimetric displacements, allowing accurate adjustments of optical elements and other system components. Two different movable stages were used in this project. Both feature one or more rotating knobs that produce small displacements and sub-millimetric scales that allow the quantification of these displacements.

In order to allow the minute lateral displacements with no vertical change necessary for the directionality measurements, the 1.59 mm diameter optical fibre used as the light source was fixed in a holder attached to a long one-dimensional movable stage.

The bite-bar was fixed on a three-dimensional movable stage allowing the precise adjustment of the eye position in all three directions.

Mydriatic Eye drops:

Mydriatic drugs are substances used to maintain a dilated eye pupil by blocking the neurotransmitter receptors responsible for pupil constriction or by stimulating the ones responsible for pupil dilation [34]. At a certain stage of the project pupil dilation with tropicamide 1% was used with the goal of increasing image resolution.

Optical Power Meter:

An optical power meter (OPM) was used throughout the project to measure the power of light delivered to the eye before any experiment. It basically consists of a calibrated sensor with an amplifier and two displays: one analogue, other digital.

The OPM used was a *Thorlabs PM30-130*, which is able to measure optical powers from 5 nW to 500 mW with wavelengths between 400 and 1100 nm. Before any measure, the average wavelength of light being used in the system must be specified, therefore, when using the red filter the wavelength chosen was 650 nm; likewise, if the green filter was being used the wavelength would be set to 550 nm.

7. System Development and Experimenting

In this project, two main approaches were attempted at the goal of imaging the retina: the first of those makes use of a Maxwellian illumination method, while the second uses a small diameter optical fibre in front of the eye as the light source. Images of the development of the setup are presented in appendix A.3.

In a first phase of the project the implemented setup was divided into two systems: the illumination system and the image formation system, just like a standard fundus camera. However, the illumination system differed in that it consisted of a Maxwellian view illumination method, in which a minified image of the light source is produced at the pupil plane by use of a positive lens and a means to reflect it towards the eye.

The 1.59 mm diameter optical fibre was used as the light source. This was followed by an achromatic doublet lens at its focal distance to render the light waves plane and another achromatic doublet then followed to produce the image of the source. The light beam was then deviated 90º towards the eye by the beam splitter.

After exiting the eye, the light would enter the imaging system. The beam splitter may therefore be considered as part of this setup as well, since light would pass through it before reaching other refracting elements. Those elements consisted of two achromatic doublet lenses arranged in a telescope disposition and a third doublet lens which produced a final image.

This was the initial setup, several modifications and improvements were made to this.

The first of those was to substitute the two lenses that followed the light source by a single lens. This allowed a reduction in the amount of light lost in surface reflections and also in the size of the illumination spot. First, an achromatic doublet lens of 50 mm focal length was used and then a 35 mm biconvex lens. The first of those required a considerable distance from the source in order to produce a small illumination spot, resulting in a substantial loss of illumination. The 35 mm lens allowed the production of a 1 mm image of the source on the pupil plane while gathering a considerable amount of light. An aperture of controllable diameter was also used between the source and the lens in order to better control the shape of the illumination spot.

After some trials using a simulated eye made of a 19 mm achromatic doublet followed by a paper one focal distance away with an arrow drawn on it with graphite, and a white paper as a screen, it was concluded that the telescope arrangement was not necessary and the removal of the last two lenses could actually improve the image by reducing the amount of light lost by surface reflections, so that only the long focal length lens (300 mm) of the telescope was left in the setup.

At this stage of development the image sensor was installed in the setup and connected to the computer and screen. Good images of the graphite drawn arrow were obtained, one such example is shown in figure 7.1. Nonetheless, the 19 mm lens and paper substituting the eye were far from simulating a real eye: the paper used was white paper with a reflectivity of about 90%, the lens diameter was 127 mm and it presented hardly any aberrations, whereas the reflectivity of the retina is about 0.1%, the pupil diameter 5 mm with a medium aperture [34] and the aberrations of the eye are much greater. The results obtained with the eye were therefore not satisfactory, with the occasional visualization of a large blood vessel. White light directly from the source was shortly used on a first attempt. A red filter was then installed following the source and used through most of the project, in order to increase the subject's comfort and to take advantage of the higher reflectivity of the retina in the red light bandwidth.

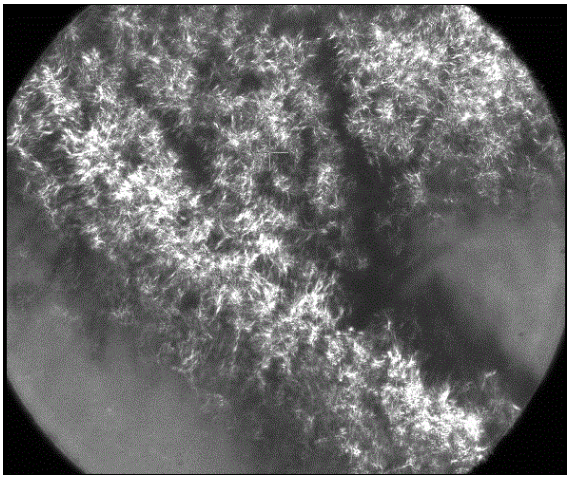

Figure 7.1 Image of the graphite arrow drawn on paper, obtained with the imaging setup.

A possible reason for the poor results obtained was attributed to an existing amount of stray light that contributed to a high background on the image formed. At this point, the illumination section of the setup was isolated from the rest by black card and a black cloak covered the whole system in order to reduce unwanted light. In addition to this, the lights were turned off in the laboratory during the acquisition. Nonetheless, a considerable counting of photons was obtained just by turning the light source on. Therefore, further isolation of the several elements was done using black card and tape. Another controllable aperture was put in front of the beam splitter, followed by a "tunnel" made of black card with its end on a hole made on a card wall that created an isolated compartment where the subject's eye laid. Figure A.2 shows a photograph of the setup. The 300 mm focal length lens was also substituted by a 200 mm lens and placed so that both the sensor and pupil of the eye lay in conjugal planes.

After substantial reduction of the amount of stray light was achieved, new images were acquired. These were still very poor in quality, allowing only a few visualizations of a larger vessel and only one brief visualization of the branching of minor vessels. The lack of quality of the images was attributed to a significant reflection of light by the cornea, since images of the eye at a distance from the correct plane, showed a bright circular shape with photon counts

close to those of the attempted images of the retina; this circular shape corresponds to the cornea.

The beam splitter was also a major source of unwanted light reflection into the sensor. In order to remove these reflections, the beam-splitter was replaced by a semi-circle mirror which reflected half of the illumination beam into eye while allowing light coming from the retina to travel through the space where there was no mirror. Illumination was nonetheless uneven and poorer image quality was obtained.

Optical Fibre

At this point of the project a new strategy was adopted: the 0.73 mm diameter optical fibre was used as a light source to directly illuminate the retina. The previous thicker optical fibre was removed along with the 35 mm lens and the beam splitter. In this new configuration, the optical fibre was placed as close as possible to the eye by using a thin plastic coverslip with a hole at its centre smaller than the cladding of the fibre but larger than its core, therefore, by removing the cladding of the fibre the coverslip could be used to hold it. The coverslip was secured on a movable stage with a millimetric knob to allow for fine adjustment. Behind the coverslip lay an iris and a black card tunnel that entered a card wall ensuring an efficient shielding of stray light. The fibre was bent away from the imaging path avoiding any shadows. Like in the previous setup, a 200 mm focal length lens laid between the eye and the sensor.

This new approach had the advantage of using all the light that comes from the retina, since no beam splitter or other reflecting element is required. In addition, since the illumination source was so close to the eye, the imaging light shared a very short travelling distance with the illumination light, reducing greatly any interference between both light beams. Corneal reflections were also reduced.

Good results were obtained using a simulated eye and are shown in figure 7.2, this time the white paper on the simulated eye was substituted by a black and white target.

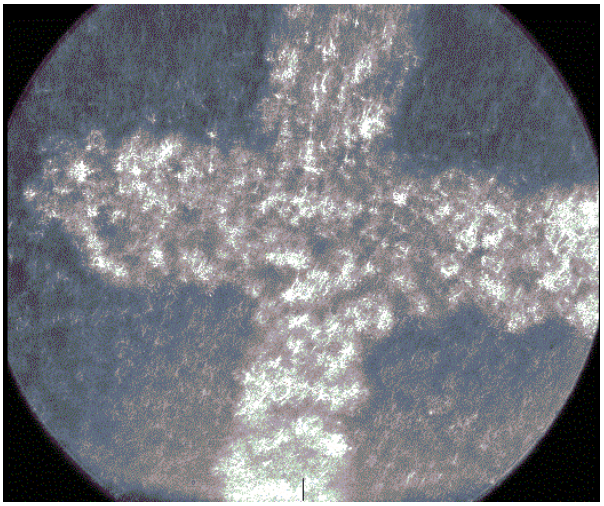

Figure 7.2 Image of the target used to simulate the retina, obtained with the thin optical fibre setup.

Despite its advantages, this new approach proved to be unpractical due to the close proximity of the eye to the optical fibre, which not only caused discomfort to the test subject but it also posed a risk of eye infection if contact were made between the eye and the fibre.

To counter such complications, a 19 mm focal length lens just like the one used to simulate the eye was used between the fibre and the eye, conveying greater safety and comfort to the test subject. Nonetheless, this lens was too small in diameter to capture a decent amount of light coming from the retina, being incapable of producing any images, not even with the simulated eye. In order to increase the amount of light gathered from the retina, a biconvex lens with the normal diameter and 25 mm focal lens was used instead. However, the use of this lens implied the placement of an iris between the fibre and the lens itself, in order to produce a focused illumination spot on the pupil. This iris in turn reduced considerably the light coming from the eye, providing no advantage at all.

As a further attempt to increase light relayed to the sensor, the 200 mm focal length lens was replaced first by a 50 mm and then by a 60 mm focal length lens which were placed closer to the aerial image formed by the 19 mm lens. This close distance also implied a considerable proximity between the lens and the optical fibre, which resulted in significant gathering of light from the tip of the fibre itself and the production of a substantial shadow by the body of the fibre, excluding completely this possibility. In face to the lack of lens with focal lens between 60 and 200 mm, lens combination was also attempted with no success.

Back to Maxwellian View

Considering the difficulties presented by the optical fibre approach, the idea was put aside and the previous setup was reassembled, with slight differences in distances and shielding.

The 1.59 mm optical fibre was placed in a holder installed on a millimetric movable stage, to allow for its lateral displacement in a more advanced point of the project. The iris diaphragm was set to its smaller diameter possible: approximately 1.5 mm, and placed approximately 3 cm away from the fibre. A positive lens with 50 mm focal length was placed 13 cm away from the iris diaphragm and used as the Maxwellian lens, producing a minified image of the source 7.3 cm away which was deviated by the beam splitter onto the pupil. A positive lens of 300 mm focal length was placed so that the eye pupil and the sensor lay in its conjugate planes, i.e. each within 300 mm from the lens. Since this lens formed a retinal image by focusing the plane wave coming from the eye, it may be called imaging lens.

This lens was inserted in a black card wall that separated the sensor from the illumination optics and the eye. Another taller card wall was placed between the light source and both illumination and imaging systems. No further shielding was used at this stage, nonetheless, the first images with reasonable quality were acquired, allowing the visualization of large and smaller blood vessels, and some nerve fibres as well, with a magnification given approximately by the ratio between the focal length of the achromatic lens used and the focal length of the eye (considered to be 17 mm): 300/17 = 17.6, one such exemplary image is shown in figure 7.3.

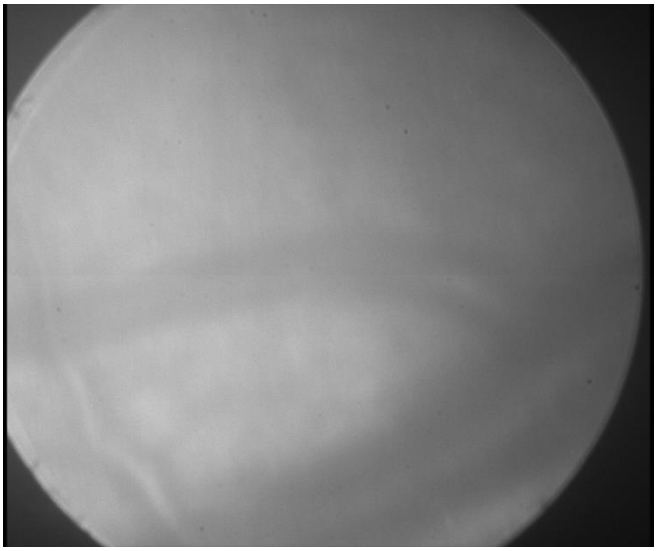

Figure 7.3 One of the first images with a visualization of blood vessels, acquired with 0.5 s exposure and 17.5 μW irradiance.

Once consistent visualization of blood vessels was achieved, the next step was to increase magnification in order to visualize the cone photoreceptors. For such a purpose, the sensor was moved further away from the imaging lens and an achromatic lens of 50 mm focal length was placed between the two. This lens was used to focus on the aerial image produced by the imaging lens and relay it to the sensor with a magnification that could be changed by moving either the sensor or the lens itself. It may therefore be called the zoom lens.

A trail for both the zoom lens and the sensor was mounted in the table in order to make it possible to change zoom and focus by moving both elements, while maintaining system alignment. By moving both the zoom lens and the sensor by equal amounts, the magnification could be kept approximately constant while the focus of the image was progressively changed. Once good focus was achieved, magnification could be increased with little change on the focus of the image by moving the sensor away from the zoom lens. Small adjustments to the focus could be performed by approaching the zoom lens to the aerial image, which also increased the magnification.

There was no need for considerable magnification in order to obtain the first visualizations of possible cone photoreceptors, those are shown in figure 7.4. Those structures were far apart from one another and were quite large, especially considering the fact that the magnification was only slightly increased; one may therefore conclude that if those structures were cones its visualization occurred at great retinal eccentricities, where cones have larger diameters and are farther apart than in the fovea or parafovea [37].

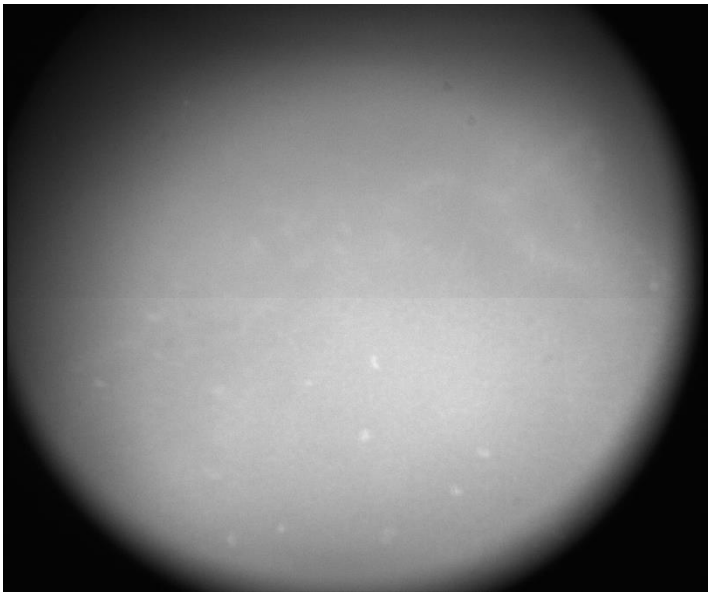

Figure 7.4 First visualization of possible cone photoreceptors at large eccentricities, those moved consistently across the screen as the subject moved her eye; acquired with 0.3 s exposure and 24 μW irradiance.

In order to achieve the visualization of parafoveal cones, image contrast needed to be increased. This was accomplished by adding a linear polarizer after the light source and another linear polarizer after the imaging lens. This approach exploits the birefringent nature of the eye: linearly polarized light entering the eye will exhibit elliptical polarization when leaving it [34]; by setting the polarization axis of each polarizer perpendicular to one another, the only light that will pass the second polarizer will be the component of light coming from the retina with a polarization axis parallel to the this polarizer axis, light coming from reflections on the beam splitter and other surfaces is greatly reduced. This approach also implies a greater demand of power from the light source.

The use of polarizers enhanced the contrast of blood vessels, as shown in figure 7.5; nonetheless, the fundus lost detail and neither the cones nor the nerve fibres could be visualized with reasonable quality, probably due to the reduction of the amount of light contributing to the image.

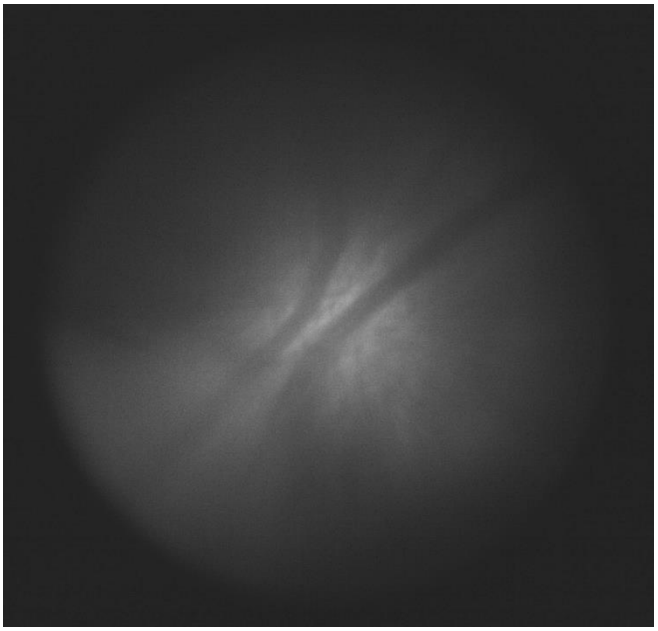

Figure 7.5 Increased vessel contrast using the polarizer filters, acquired with 0.1 exposure and 20 µW irradiance. Reduced availability of light is made obvious.

At this point of the project a minor improvement was done in the setup: the whole system was raised in order to provide greater comfort for taller test subjects and part of it was put onto a platform which extended the system outside of the optical table, enhancing comfort as well.

Diffraction by the eye pupil was still a possible limitation on the quality of the images; therefore, mydriatic eye drops were used to maintain a large pupil in an attempt to increase image resolution. A slight increase in resolution was observed and it was just enough to allow the first visualization of the parafoveal cone mosaic with reasonable quality, one of the images obtained at this point is shown in figure 7.6. Nonetheless, good images of the cone mosaic were posteriorly obtained without recurring to mydriatic eye drops.

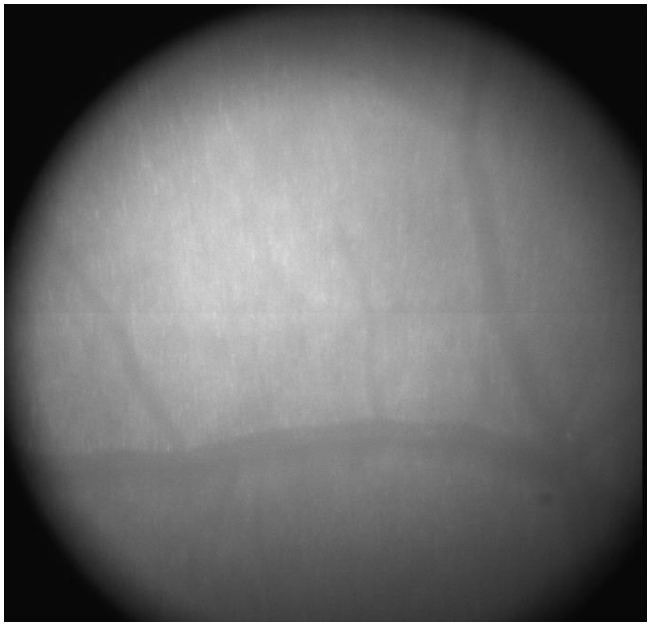

Figure 7.6 One of the first images of the parafoveal cone mosaic obtained, acquired with 0.05 s exposure and 20 µW irradiance. The minute cones are visible among the vessels.

Two final resorts were attempted with the aim of improving image quality: a green filter and an optical shutter. For reasons already presented in the text, the use of green light is often preferred when imaging the cones; in the absence of a green light source, a green filter was used. In order to maintain the test subject's comfort and safety, a lower source power was required while imaging the retina, due to the higher sensitivity of the eye for green light. Such reduction of the light available in the system, resulted however in a reduction of image quality. In order to reconcile high power levels and subject's safety, a shutter was used to limit the amount of time during which the eye is exposed to light. Exposure times between 1 and 3 seconds were used, and reasonable results were attained. Nonetheless, no considerable improvement was observed and the use of a green filter was excluded.

The optical shutter found nevertheless a second application: allow the use of high light power levels to obtain videos with a high frame rate, reducing motion artifacts and ultimately improving image quality. Exposure times between 1 s and 10 ms were used either by triggering the opening and closing of the shutter manually or by synchronizing it with the software. Synchronization with exposure times of less than 50ms proved to be unfeasible, due to a delay between the acquisition by the sensor and the opening of the shutter. Manual triggering of the shutter yielded reasonable results by setting the shutter to an exposure time of 1 second and using exposures times between 0.09 and 0.01 seconds in the sensor (with light irradiances between 30 and 100 µW respectively), producing 1 second videos with different frame rates. Surprisingly, no considerable improvements were observed and the method proved to be less practical, since it did not allow the free exploration of the retina for longer periods of time, and the sudden opening and closing of the shutter prompted a reflex in the subject which resulted in a considerable displacement from the region to be imaged. The idea was therefore discarded.

At this point, continuous experimentation with different magnification values and focusing planes was done with exposure times around 0.1 seconds, in order to find the conditions which provided optimum image quality of parafoveal cone photoreceptors.

8. Final Setup and Directionality Measurements

Once good images of the cone mosaic were consistently obtained, the magnification, focusing plane and exposure time were fixed and the directionality measurements were finally undertaken.

In the final setup, the Maxwellian lens formed an image of the optical fibre with a 0.46 magnification (a minified image) on the pupil plane. The zoom lens and sensor were fixed to the optical table at such distances that the total magnification produced was approximately 11.5 times. This means that the zoom lens actually reduced the magnification provided by the imaging lens and the eye lenses; although a superior magnification would be desirable, it would require the use of higher irradiance levels which would compromise the health and comfort of the test subject, nonetheless the magnification provided by the system proved to be enough to allow visualization of the cone mosaic with enough quality to proceed to the directionality measurements. Greater magnification would also imply increased motion artefacts and aberration effects.

The exposure time chosen for the measurements was 0.1s. This choice made it possible to use relatively low irradiance levels (around 25 µW) while keeping motion artefacts low and allowing the production of short videos, instead of single images or extremely short videos. These videos were desirable to guide the test subject's stare into the right position, so that the same region of the retina could be consistently imaged at all the pupil entrance positions for the light, while producing a set of images from which those with best quality could be chosen. A red filter was used rendering the wavelength bandwidth of light around 650 nm. The measurements were performed at approximately 15º retinal eccentricity.

The optical elements which would not be used in the final measurements, such as the polariser filters and the optical shutter, were left in the setup in such a way that they could be easily added and used in the system in a posterior application. The same applies to the trail mounted for the zoom lens and the sensor; even though these two optical elements were now fixed to the table, they could be easily unscrewed from the table and slid along the trail to change focus/magnification.

A schematic representation of the final setup follows in figure 8.1, along with a table with the distances between the optical elements, table 8.1. Only the elements used in the directionality measurements are represented: the light source illuminates the system through the optical fibre which is fixed on the millimetric movable stage and scale; this is then followed by the red filter, iris diaphragm, Maxwellian lens and beam splitter; after leaving the eye (black dashes), light is focused by the imaging lens forming an aerial image which is focused on the sensor by the zoom lens; the sensor is finally connected to the desktop computer allowing visualization. Photographs of the final system are also shown in appendix A.4.

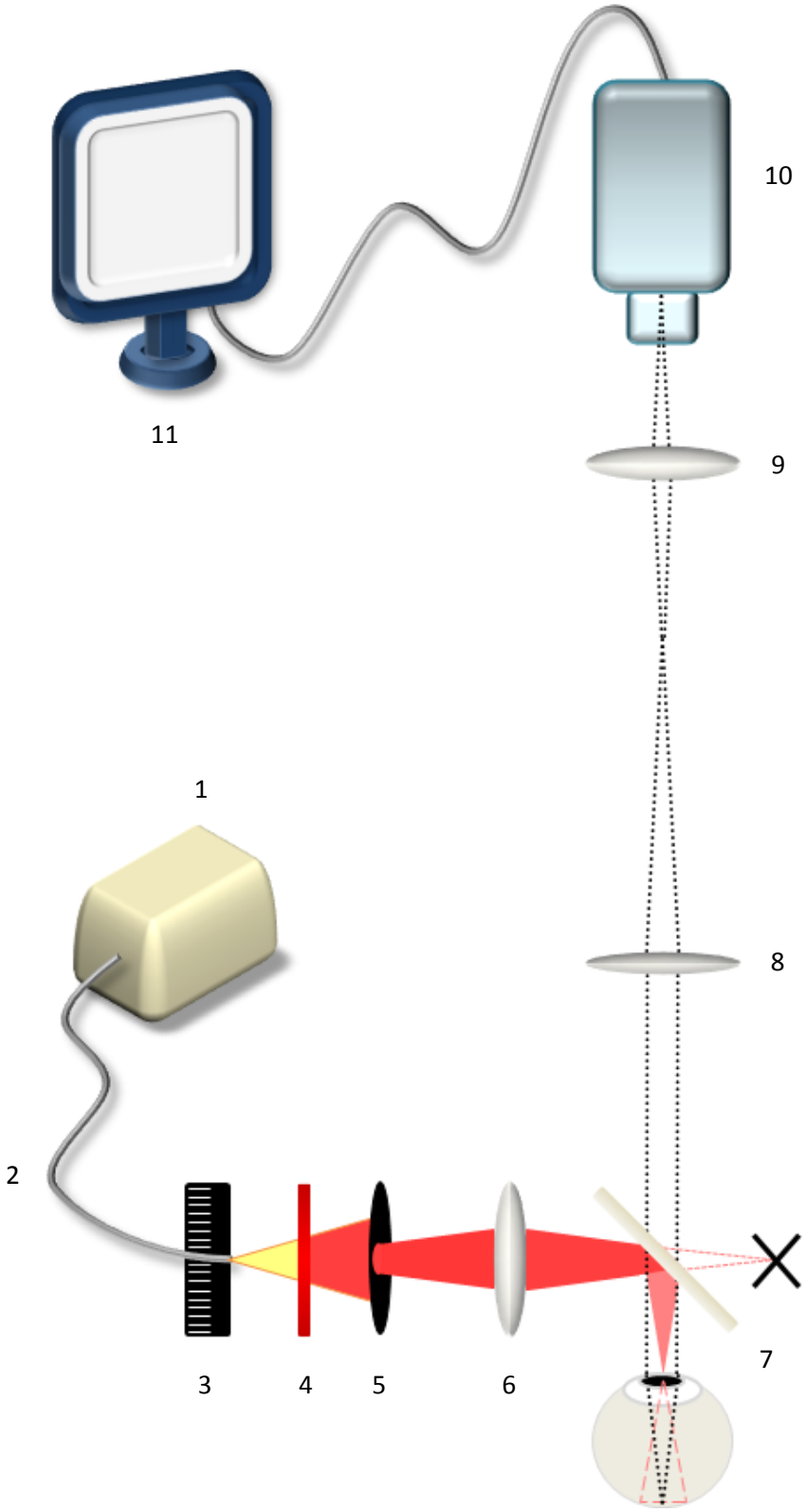

Figure 8.1 Diagram of the final system. 1 – Illuminator; 2 – Optical Fibre; 3 – Millimetrical Stage; 4 – Red Filter; 5 – Iris Diaphragm; 6 – Maxwellian Lens; 7 – Beamsplitter; 8 – Imaging Lens; 9 – Zoom Lens; 10 – Sensor; 11 – Desktop Computer.

Table 8.1 Distance from each element in the system to the previous one. The lenses focal length, the diameter of both the iris diaphragm and the optical fibre and other information is also provided.

	Distance (cm)	Info
Optical Fibre	0	Ø = 1.59 mm
Iris Diaphragm	3	Ø = 1.5 mm
Maxwellian Lens	13	f = 50 mm
Beam Splitter	5.6	50:50
Eye Pupil	1.7	2 mm < Ø < 8 mm
Imaging Lens	30	f = 300 mm
Zoom Lens	35.5	f = 50 mm
Sensor	8.3	2560 x 2160 pixels

The method used to perform the directionality measurements in the test subject's right eye is now outlined:

1. The light source is aligned with the Maxwellian lens using an alignment target.
2. The subject's eye is carefully positioned and aligned with the illumination beam.
3. Once aligned, the illumination beam is displaced laterally in the temporal direction (away from the nose) so that the illumination beam is occluded by the subject's iris.
4. The beam is slowly displaced nasally until the subject starts seeing the beam circle completely. This will be the first entrance position of light in pupil.
5. The subject is asked to look in the direction of the LED used to maintain the chosen region of the retina under the field of view of the camera, but to keep focusing behind it.
6. A 9 seconds video of the selected region of the retina is made.
7. The optical fibre is displaced 0.5 mm which translates to an approximate 0.2 mm nasal displacement of the illumination beam in the pupil.
8. A new 9 seconds video of the same region in retina is made.
9. Steps 7 and 8 are repeated until the subject starts seeing the beam occluded by the iris in the nasal side.

9. Results

The main goal of the project was the study of the directionality of the retinal cone photoreceptors using imaging; therefore, the visualization of these structures constitutes a goal in itself. Hence, two types of results may be distinguished: retinal images and directionality measurements.

Two test subjects participated in the experiments providing these results: Salihah Qaysi and the author. Both participants had no ocular pathologies; participant Salihah Qaysi had no significant refractive error while the author required -2.5 Dioptre refractive correction.

9.1 Retinal Images

In this section, multiple images obtained during the development of the system and after its conclusion are shown. Even though the photoreceptors constitute the structures of main interest to the project, several different structures of clinical interest were also visualized. Most of these images were obtained from the right eye of the test subject Salihah Qaysi, some were obtained from the author's right eye and an indication will be given when this is the case. The wavelength bandwidth of light used was around 650 nm (using a red filter), the irradiance was kept below 30 µW and the illumination duration below 30s at all times, well below the safety guidelines shown in appendix A.1. Most images shown here display 11.5 times magnification and a field of view of 5º; considering the fact that those of the parafoveal cone mosaic were acquired at retinal eccentricities close to 15º and that cones have diameters of approximately 8 µm at such eccentricities [12], the image resolution may be estimated to 8 µm, since cones are the smallest discernible structures in the images.

9.1.1 Optic Disc

With its large circular shape, high reflectivity and branching of large blood vessels, the optic disc is an easily identifiable structure while imaging the retina. Due to the relatively high magnification used during the project, no images of the whole disc were obtained; nonetheless, a few exemplars where the optic disc can be partially seen were acquired and are shown in figure 9.1.

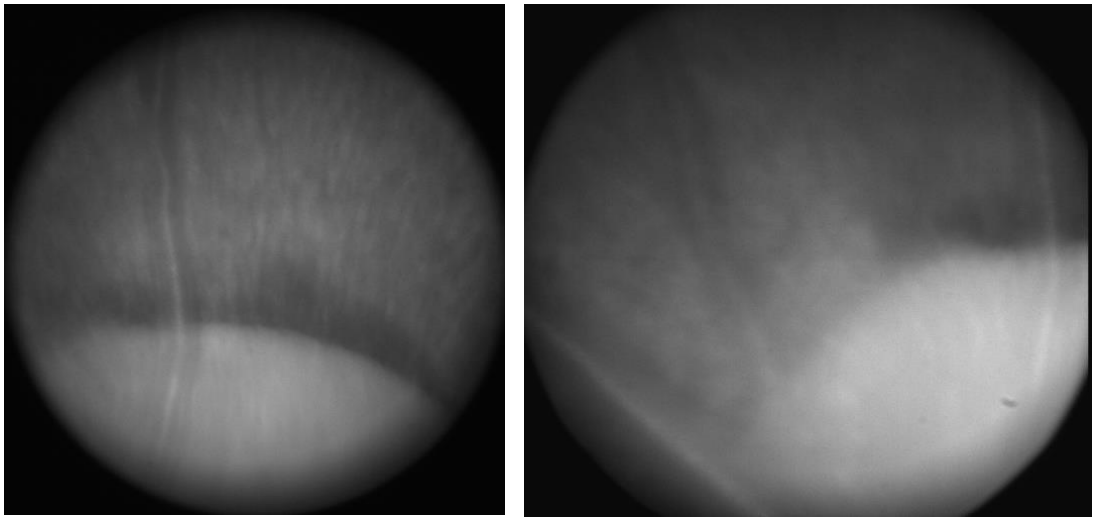

Figure 9.1 11.5 and 12 times magnified images of sections of the optic disc. The nerve fibre layer is also visible in the first image.

9.1.2 Blood Vessels

The most frequent sighting while imaging the retina is blood vessels, another structure of the retina with major clinical importance. In figures 9.2 and 9.3 some exemplary images of large blood vessels are shown.

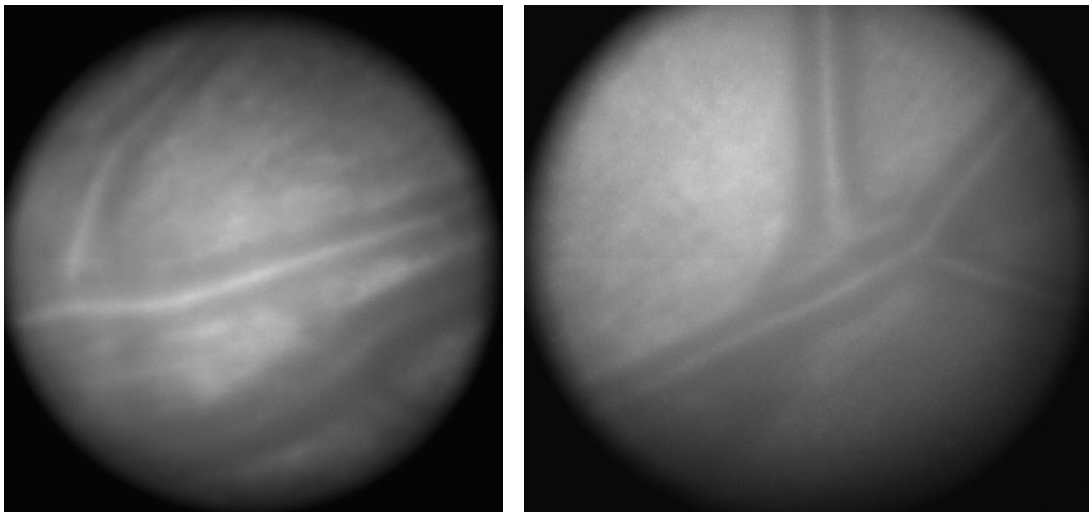

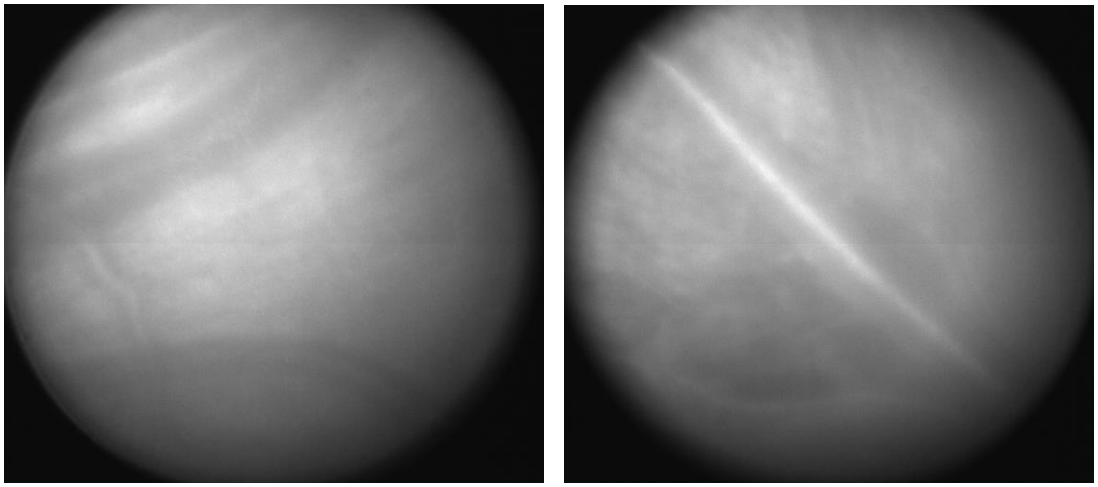

Figure 9.2 Set of 4 images of large blood vessels. Vessel crossing and vessels with different reflectance spectra may be seen. The nerve fibre layer is also visible in some of the images.

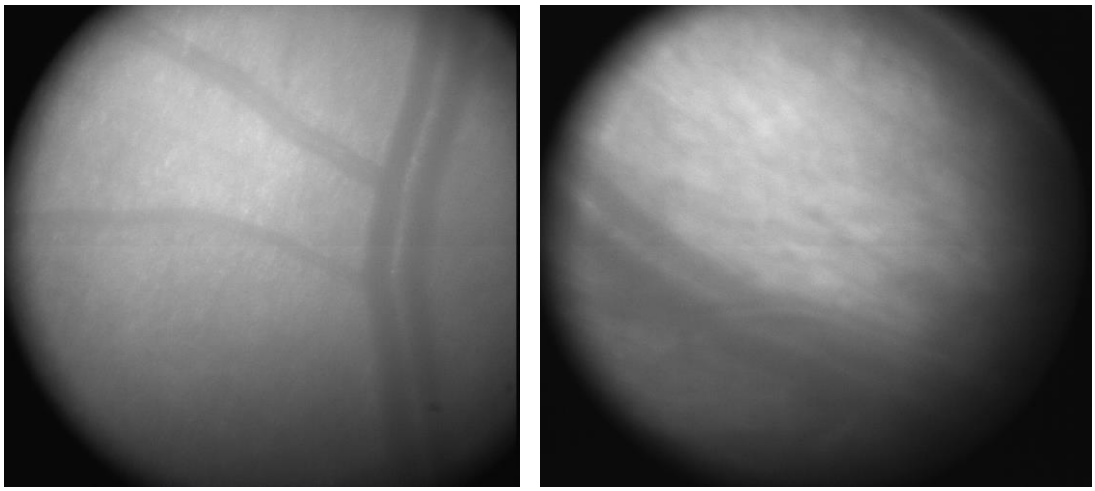

Figure 9.3 Two capillaries branching from a large blood vessel in the first image. The cone mosaic is also visible. The second image features a capillary crossing over a large vessel.

9.1.4 Capillaries and Cone Photoreceptors

Some of the best images obtained and with greater interest for the project are those which show the cone photoreceptor mosaic, in such images the capillary ramifications are usually present as well. Since these images benefit from a larger dimension in order to improve the visualization of parafoveal cone photoreceptors, they are shown in appendix A.5.

9.1.5 Digitally Enhanced Images

Apart from cropping, all images shown so far have suffered no digital processing, they are shown as they were acquired. The same applies to those shown in the appendix.

In this section of the results, figures 9.4 to 9.6 show a few images after being digitally enhanced through simple technics.

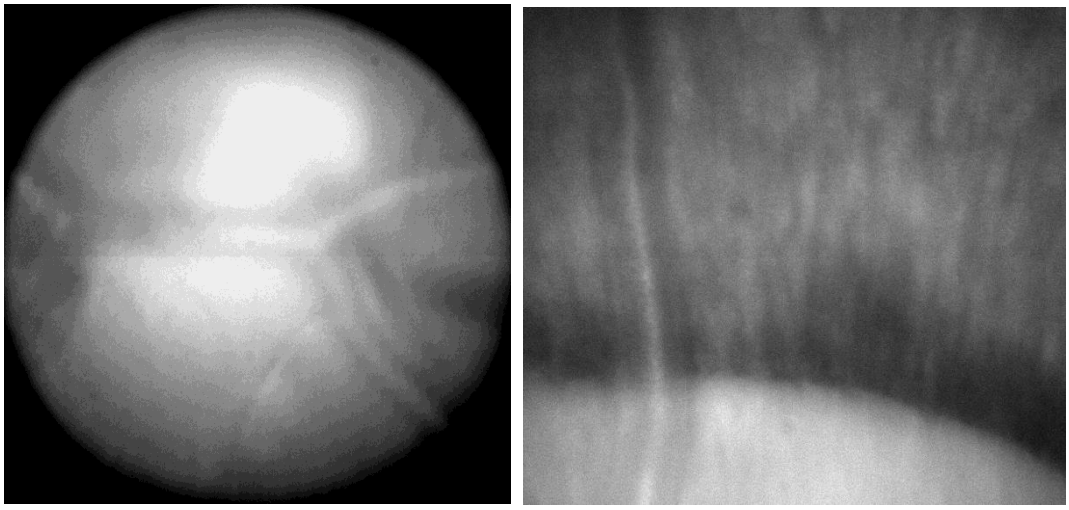

Figure 9.4 On the left, an image of the center of the optic disc is shown. Due to the high reflectivity of the disc, the image brightness had to be reduced and its contrast adjusted. On the right, a section of the image shown in figure 9.1 with an optimized contrast.

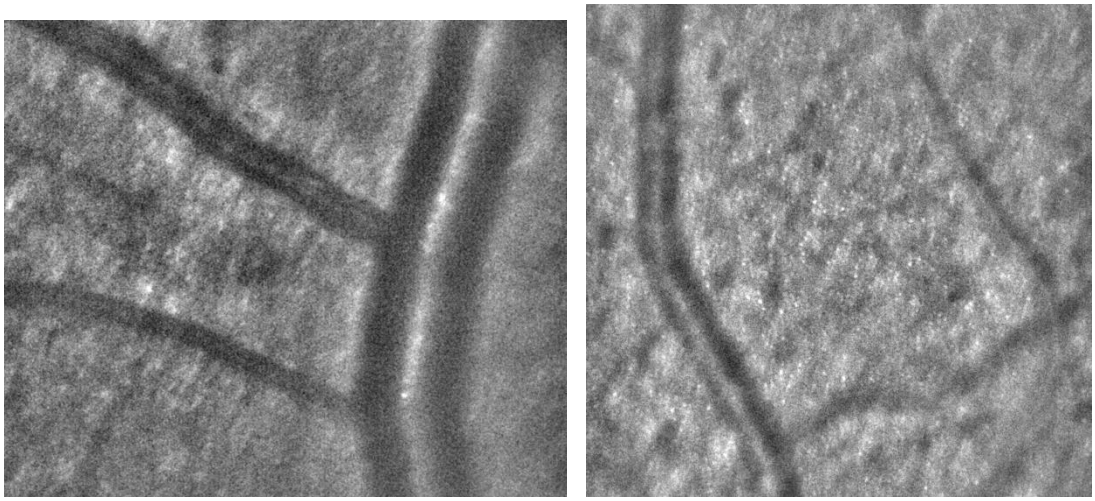

Figure 9.5 Two segments of retinal images which were subject to a Fourier band pass filter, with a lower limit of 2 pixels and an upper limit of 180 pixels, smoothing slightly the image, enhancing brightness uniformity and removing an acquisition artefact caused by the sensor consisting of a straight line crossing the whole image horizontally. Contrast optimization through histogram equalization followed. Cone photoreceptors are visible in the center of the second image.

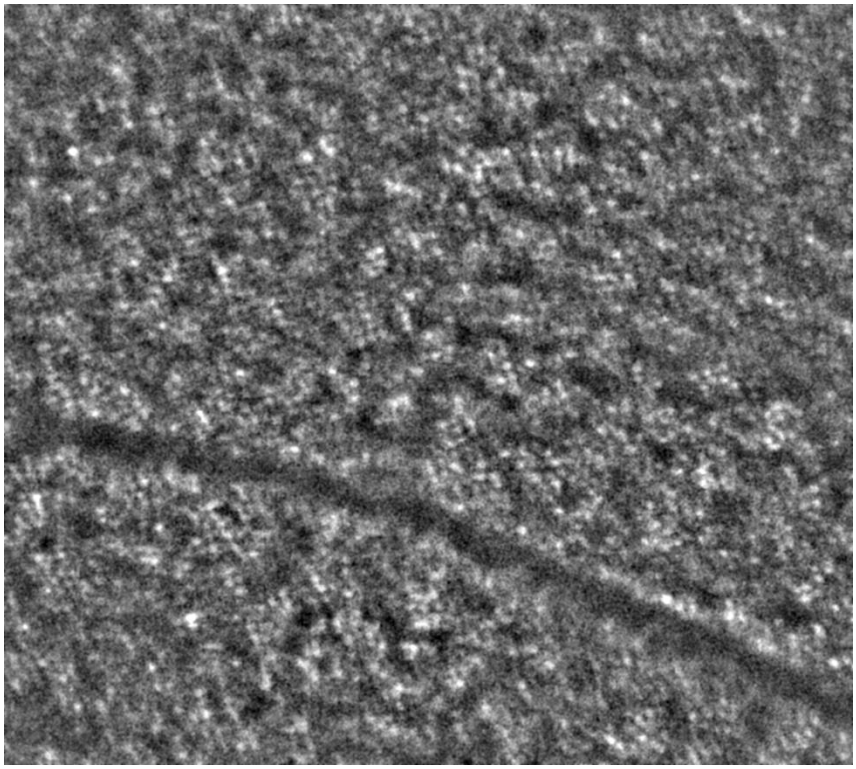

Figure 9.6 Central segment of figure A.14 after a similar treatment as the previous pair of images. Individual cones are clearly visible all across the image.

9.2 Directionality Results and Analysis

Three scannings of the participant's eye pupil were performed: two on a non-dilated pupil and one in a dilated pupil. At the end of these, three sets of between twelve and fourteen 9 seconds videos were obtained. The following procedure was used to analyse the videos:

1. 50 images were extracted from each video.
2. 10 of these images were chosen based on illumination uniformity.
3. For each of these images, the mean brightness of a square of 300 pixel side was measured always in the same place using vessels as reference.
4. Once all 10 images from one video were thus measured, the mean value of this set of values was calculated.
5. After repeating the process for all the videos in each scanning, all the mean values obtained were normalized, its logarithm was calculated and the resulting values plotted against its respective entrance points in the pupil.
6. Finally, the data was fitted to a parabola to allow further analysis.

The final results are now shown in figures 9.7 to 9.9; blue points represent calculated values while the black line represents the parabola fitting curve, respective R^2 values are also shown.

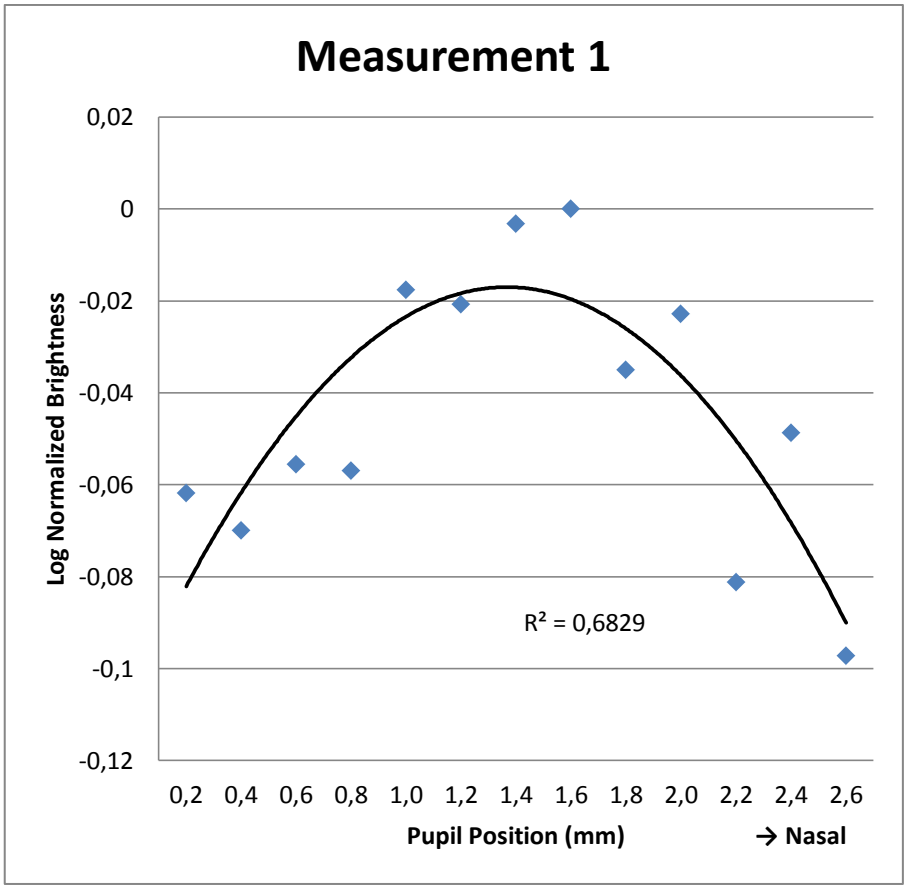
Measurement 1
0,02
0
-0,02
-0,04
-0,06
-0,08
-0,1
-0,12
Log Normalized Brightness
R² = 0,6829
0,2 0,4 0,6 0,8 1,0 1,2 1,4 1,6 1,8 2,0 2,2 2,4 2,6
Pupil Position (mm)
→ Nasal

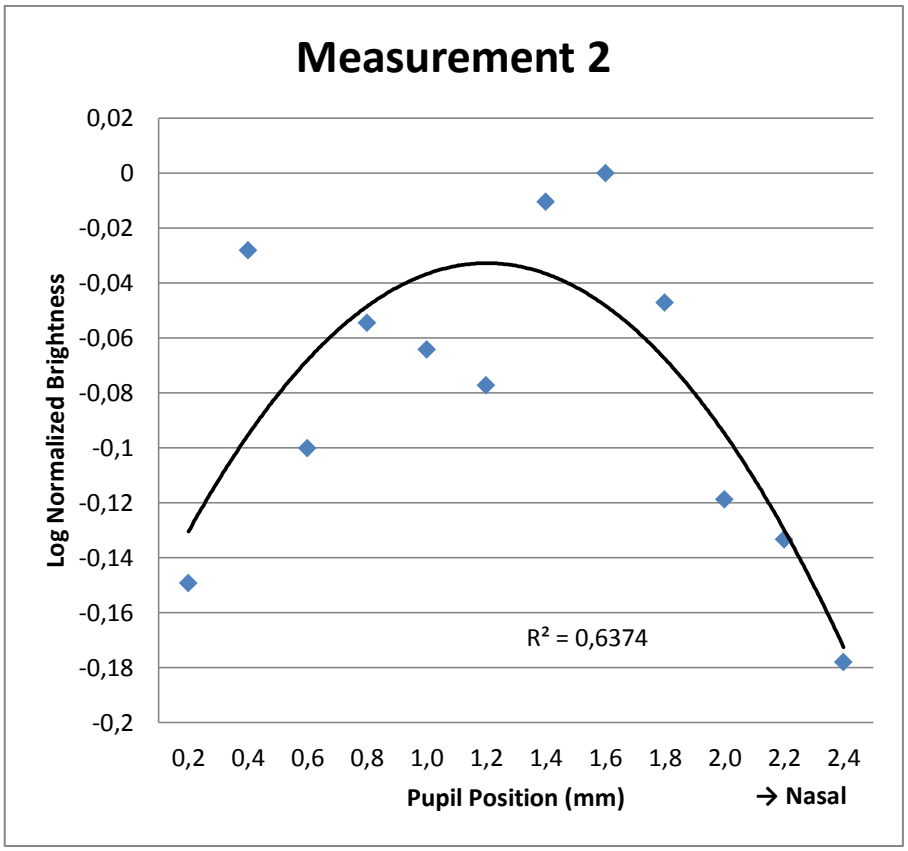
Measurement 2
0,02
0
-0,02
-0,04
-0,06
-0,08
-0,1
-0,12
-0,14
-0,16
-0,18
-0,2
Log Normalized Brightness
R² = 0,6374
0,2 0,4 0,6 0,8 1,0 1,2 1,4 1,6 1,8 2,0 2,2 2,4
Pupil Position (mm)
→ Nasal

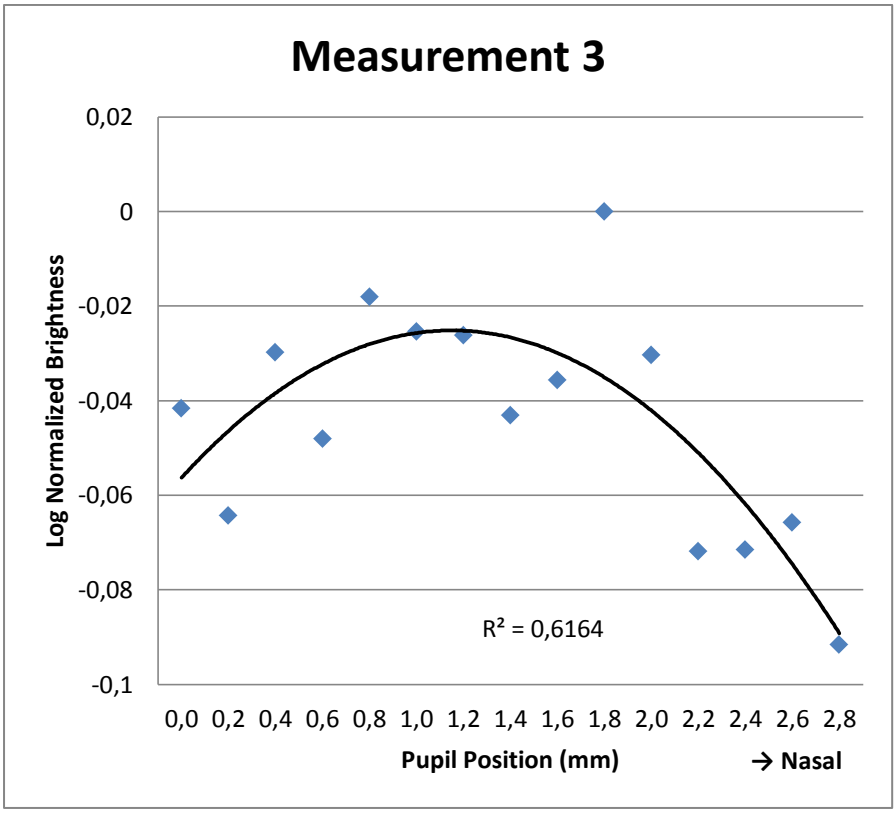

Figures 9.7 to 9.9 Results of the directionality measurements.

The final results obtained from the directionality measurements show the expected parabolic trend characteristic of the Stiles-Crawford effect. Nevertheless, a marked variation of the brightness is easily noticeable and as a consequence the best curve fit shows an R^2 value of 0.6829. The observed variations in brightness may be explained by a number of factors.

First of all, the pre-amp gain of the sensor may be responsible for changing the photon counts of the pixels from one image to the other depending on illumination conditions. This means that this gain is not constant and while a certain amount of photons produces a certain brightness in one image, it may produce a different brightness in another image in order to maintain dynamic range.

Another source of variations resides in the way the illumination beam was mounted and moved across the pupil. As the point of light entrance changes, so does the illuminated region of the retina, this means that the subject must move the fixation point in order to keep the same region of the retina under illumination. As a result, in some images the region of interest will be right under the illumination beam, while in others it will be slightly displaced, originating variations that undermine the accuracy of the results. Additionally, the field of view of the camera is kept unchanged, therefore, the field of view will not match the illuminated region as it changes. As a consequence, an increasingly darker region of the retina starts being imaged, precluding directionality measurements across dilated eye pupils.

Optical aberrations, corneal reflections and other factors already discussed also contribute to the production of inaccurate results.

On the other hand, the fact that the Stiles-Crawford curve is usually measured through a dilated pupil should also be considered, this means that a length of approximately 8 mm is scanned, whereas in the present study only a section of this curve was obtained, therefore, by enlarging the length of the scanning the variations would fade and the standard deviation of the normalized brightness would be reduced. The last set of results shown here (measurement 3) was obtained from a dilated pupil; however, these could not be performed to its whole extent due to reasons already discussed.

10. Discussion and Conclusion

The present project set out to develop a fundus camera using simple optical elements, and use this camera to study the photoreceptor directionality in the healthy human retina. This well-known phenomenon, known as the Stiles-Crawford effect, is characterized by a Gaussian dependence of the change in brightness perception with the position of light entrance in the pupil, and it is altered in a number of ocular pathologies. While fundus imaging is a well-established clinical practice, its use in the assessment of retinal directionality outside the academic sphere is still taking its first steps. Its widespread use in the clinical environment would represent a significant improvement in the health technology.

The first challenge presented in this project consisted of devising a way to obtain retinal images of the cone mosaic by assembling a light source, lenses and an image sensor device.

Direct illumination of the eye using a thin optical fibre cobbled to a light source was attempted with no success: the proximity between the fibre and the eye required to obtain reasonable images posed a risk for the health and safety of the participant, a more advanced device would be required to assure no contact occurred between the cornea and the fibre, such device could incorporate a camera or distance sensor which along with a precise robotic or manual arm could place the fibre at a safe distance from the cornea; participant's head movement would also have to be completely eliminated. Maxwellian illumination was therefore the preferred method to illuminate the retina: by using a larger optical fibre, one lens and a beam splitter a simple method was conceived to deliver light to the eye fundus. This approach provided a uniform illumination field in the retina and a very minute illumination spot on the cornea in a safe way while still making it possible to change the entrance point in the pupil. An iris diaphragm was also necessary to control the illumination spot size and reduce its aberrations and the use of a red filter was found to be of advantage by increasing the participant's comfort while availing of the increased retinal reflectance on the red wavelength bandwidth of the spectrum. The beam splitter was necessary to deflect the illumination beam towards the eye while keeping the light source, lens and the other elements out of the way of the eye. This was a 50:50 beam splitter, which meant the light intensity produced by the system was halved before it reached the eye and halved again after it left the eye while making its way to the sensor, a significant reduction on the amount of image forming light was thus inflicted. Nonetheless, the alternatives proved unpractical: a high reflectance mirror was used to reflect half of the illumination beam to the eye while allowing half of the image formed to reach the sensor, although theoretically possible this method did not produce any reasonable images, probably due to the fact that it was attempted on an early stage of the development, later attempts could have proved the feasibility of the method. Another possible approach would be to use an annular mirror which would reflect the periphery of the beam towards the eye while allowing the whole image of the retina to reach the sensor by traversing the centre of this ring. The ring would have to be elliptical in shape, due to the 90º angle between the illumination beam and the eye. The means to manufacture such a mirror were however not available.

To properly illuminate the eye with the illumination beam created and to retrieve an image with quality from its fundus, the intrinsic properties of this human organ had to be taken into account. The most obvious of these is the fact that the retina lies behind lenses made of live tissue whose properties, namely refractive power, are not constant. These lenses produce an image of the illuminated retina which might form somewhere between the infinite and 10 cm from the eye, by asking the participant to relax her eyesight and avoid focusing in close distances it was possible to place the image formed close to infinity and use an external lens to focus this image onto a sensor. Another property of the eye lenses that constantly changes is its surface rugosity, which is dictated by the amount and quality of the tear film covering it and drastically influences the image quality, it is therefore required that the participant blinks her eye constantly to maintain this tear film. Like any other lens, the eye lenses reflect a considerable amount of the incoming light; one of the strategies devised to overcome such inconvenience was the use of polariser filters to take advantage of the birefringence properties of the eye, although promising, this approach proved unworthy in the present setup: further study of the birefringence properties of the individual elements of the eye would be required and a more thorough development of the illumination system would be necessary to deliver a superior amount of light to the eye while maintaining the test subject's safety. A developed skill to eliminate corneal reflections by avoiding looking directly to the illumination beam was therefore required from the test subject. Finally, head motion presented a major source of image deterioration; the use of a bite-bar bar was found to be an efficient and easy way to overcome this issue. This bite-bar could be easily produced by warming a specific malleable material, ask the test subject to bite it and wait a few minutes for it to harden and acquire its definitive shape, it could then be used to maintain the subject's head stable by asking her to bite it. This strategy also allowed to precisely align the eye with the illumination beam by attaching the bite-bar to a three-dimensional millimetric movable stage.

Even though it was shown that one external lens was enough to form an image of the retina on the image sensor, it was found to be advantageous to further extend the system with at least one more lens. This lens allowed the refocusing of the retinal image, which increased image quality by concentrating more light coming from a particular point in the retina onto the same point in the sensor. It also made it possible to easily change the magnification and the focusing plane of the image by moving this lens and the image sensor away or closer to the eye. The use of a third lens was found to be unnecessary, since it constituted another source of aberrations and reflections in the system while adding no advantage at all. In addition to the lenses, an iris diaphragm could be used in between them, at the point where an aerial image is formed in order to reduce aberrations present in the image with the drawback of a reduction in resolution. However, this aerial image is formed at several simultaneous planes in between the lenses and they change slightly with time, making the task a more complicated endeavour which would require a greater in-depth understanding of the matter.

To finally acquire the images, a scientific CMOS image sensor with high sensitivity and low noise levels was used. Most images were acquired from short videos, no longer than 30 seconds in length. These videos proved to be valuable to explore the eye fundus and choose the regions of interest, contrarily to the acquisition of single images, which would yield visualizations of random regions of the fundus unless it had been explored beforehand and provided the staring point was fixed. Moreover, single acquisitions yielded mostly images with

eye motion artefacts, whereas within a short video there would always be a number of frames with no motion artefact. Increasingly shorter exposure times proved to further reduce these artefacts, nonetheless, this implied increasingly higher light irradiance levels. An exposure time of 0.1 seconds was shown to be the one with the best balance between subject's safety and image quality. Further reduction of the exposure time was attempted while making use of an optical shutter to control the span of time during which the eye was exposed to the necessarily stronger light. Although shorter exposure images were obtained, no improvement in quality was observed due to the fact that the shutter opening and closing noises produced an unwanted reaction in the subject which resulted in even larger motion artefacts; in addition, acquisition artefacts due to the poor synchronization between optical shutter and sensor were observed, such issue could be tackled by developing a dedicated software which would assure the proper synchronization between sensor and optical shutter. The *Labview* tools associated with the sensor could be used to develop such interface in a future phase of the project.

The high sensitivity of the sensor made it possible to acquire the extremely low-intensity images of the retina, nonetheless, it posed a disadvantage as well: any other source of light in the system, either reflective or emissive, would be detected by the sensor and added to the original signal prevenient from the retina. The shielding of the several parts of the system showed therefore to be a fundamental step to the acquisition of images with good quality. This step consisted mainly of isolating as most as possible the light source and illumination optics from the sensor while allowing the illumination and imaging beams to traverse the necessary paths, this implied cutting several shapes in black paper card with low reflectance, to accommodate the system design. A large black fabric was also necessary to cover the system and cut off external light sources such as the computer screen. An additional issue regarding stray light in the system was one of the half of the illumination beam which was not reflected towards the eye in the beam splitter, but traversed it instead, this beam continued ahead just to be reflected in the first surface which it encountered. This surface had to be very low in reflectance and should be turned away from the beam splitter; otherwise, when bounced off this surface light would be reflected at the beam splitter and directed towards the sensor, contributing to the illumination noise. The use of a black card at a non-perpendicular angle with the beam or a beam blocker proved to reduce this stray light, even though not completely. A beam blocker is a dark box designed to trap a light beam reducing considerably its reflection.

After a developmental period, a setup capable of producing high quality retinal images of the parafoveal cone mosaic with considerable consistency was conceived. This setup allowed the visualization of the eye fundus in real time and the acquisition of its images with optimum quality at a magnification of 11.5, a field of view of 5º and a resolution of 14 µm. This magnification could nevertheless be easily increased at the expense of less image quality, on the other hand, decreasing the magnification did not increase the field of view, it only provided a smaller image with the need for less light. High quality images of the several retinal structures, including parafoveal cone photoreceptors, were thus acquired. Further improvement in image quality would require the implementation of more elaborate elements in the setup, such as a badal or an adaptive optics module. Such module would be able to correct the natural aberrations of the human eye which impose a limit in image quality and make it impossible to take advantage of the full resolution that a dilated eye pupil provides. A

lens with a modifiable refractive power could also be used to compensate the defocus which takes place as a result of spontaneous accommodation. The development of such devices would constitute a whole project in itself. Image post processing was also undertaken with visible quality enhancement, Fourier filtering was found to enhance brightness uniformity, reduce noise deterioration and remove a horizontal acquisition artefact line, while histogram equalization allowed the optimization of contrast facilitating the discrimination of the several retinal structures. More laborious techniques such as image addition or image registration may further enhance image quality.

Once good images of the photoreceptor cones were acquired, the directionality measurements were made possible. Each of those was undertaken during a period of between 2 and 3 hours and yielded results that despite showing the expected parabolic trend also display considerable variations. Hence, the method used to execute these measurements required longer dedication and major improvement. First of all, the long period of time required to perform the measurements was far from ideal, a much faster method would be preferred to maintain the measurement conditions throughout the whole process and to avoid the test subject's fatigue. Secondly, the design of the illumination system hindered the accuracy of the measurements: as the light source was displaced laterally to change the entrance point on the pupil, the region of the retina under illumination changed as well, this was probably due to the fact that the Maxwellian lens was not displaced along with the source, a method to concomitantly displace both the source and the Maxwellian lens should be devised. Sensor pre-amp settings should also be further explored to keep gain constant and eliminate undesired compensations of image brightness. Finally, the use of adaptive optics on a dilated pupil would improve not only image quality but also the accuracy of the measurements.

The goal established at the outset of this project was thus successfully accomplished: a fundus camera was developed and consistently used to obtain high quality retinal images and to study photoreceptor directionality in the healthy retina. Retinal imaging is a wide field with relevant clinical applications, the challenge hereby presented contributed largely to a better understanding of this important science by the student and author of this thesis. Even though substantial improvement could be made to the developed setup in the situation of an ongoing project, the Stiles-Crawford effect was effectively demonstrated, showing how a simple system capable of assessing this natural feature of the human eye may be created and thus serving as a motivation to its further development and usage on the clinical environment.

11. Future Research Directions

This work serves as a starting point for a PhD project entitled: *"Exploring Photoreceptor Directionality using Quadrant Pupil Detection"* [43].

In this project, the developed setup will be modified to use a quadrant detection arrangement in which light enters the pupil near the SCE peak and reflected light from the retina is captured through four equal-sized sectors in the pupil plane from which individual photoreceptor inclinations can be computed.

The method will allow the determination of photoreceptor tilt without requiring the displacement of the incident beam across the pupil, considerably simplifying the process. In addition, numerical analysis predicts that the technique will be able to detect photoreceptor tilts of less than 1 degree in the retinal plane, demonstrating its clinical potential for analysis of retinal perturbations caused by drusen and retinal pathologies in which photoreceptor inclination is altered.

References

[1] Stiles, W. S., & Crawford, B. H. (1933). The luminous efficiency of rays entering the eye pupil at different points. *Proceedings of the Royal Society of London. Series B, Containing Papers of a Biological Character*, 428-450.

[2] Zhevandrov, N. D. (1995). Polarisation physiological optics. *Physics-Uspekhi*,*38*(10), 1147.

[3] Flamant, F., & Stiles, W. S. (1948). The directional and spectral sensitivities of the retinal rods to adapting fields of different wave-lengths. *The Journal of physiology*, *107*(2), 187-202.

[4] Snyder, A. W., & Pask, C. (1973). The Stiles-Crawford effect—explanation and consequences. *Vision research*, *13*(6), 1115-1137.

[5] Gorrand, J.M., (2006). The directionality of photoreceptors in the human retina. *Bull. Soc. belge Ophtalmol*, *302*, 215-229.

[6] Francia, G., & ronchi, L. (1952). Directional scattering of light by the human retina. *JOSA*, *42*(10), 782_1-783.

[7] Rativa, D., & Vohnsen, B. (2011). Analysis of individual cone-photoreceptor directionality using scanning laser ophthalmoscopy. *Biomedical optics express*,*2*(6), 1423-1431.

[8] Zagers, N., van de Kraats, J., Berendschot, T. T., & van Norren, D. (2002). Simultaneous measurement of foveal spectral reflectance and cone-photoreceptor directionality. *Applied optics*, *41*(22), 4686-4696.

[9] Gao, W., Cense, B., Zhang, Y., Jonnal, R. S., & Miller, D. T. (2008). Measuring retinal contributions to the optical Stiles-Crawford effect with optical coherence tomography. *Optics express*, *16*(9), 6486-6501.

[10] Applegate, R. A., & Lakshminarayanan, V. (1993). Parametric representation of Stiles-Crawford functions: normal variation of peak location and directionality.*JOSA A*, *10*(7), 1611-1623.

[11] Safir, A., Hyams, L., Philpot, J., & Jagerman, L. S. (1970). Studies in refraction: I. The precision of retinoscopy. Archives of ophthalmology, 84(1), 49-61.

[12] Packer, O., & Williams, D. R. (2003). Light, the retinal image, and photoreceptors. *The Science of Color, 2nd ed SK. Shevall, ed. Optical Society of America, Elsevier (Oxford, UK)*, 41-102.

[13] Flamant, F., & Stiles, W. S. (1948). The directional and spectral sensitivities of the retinal rods to adapting fields of different wave-lengths. *The Journal of physiology*, *107*(2), 187-202.

[14] Wright, W. D., & Nelson, J. H. (1936). The relation between the apparent intensity of a beam of light and the angle at which the beam strikes the retina.*Proceedings of the Physical Society*, *48*(3), 401.

[15] Quimby, R. S. (2006). *Photonics and lasers: an introduction*. John Wiley & Sons.

[16] Horowitz, B. R. (1981). Theoretical considerations of the retinal receptor as a waveguide. *Vertebrate photoreceptor optics*, *23*, 219-300.

[17] Stiles, W. S. (1937). The luminous efficiency of monochromatic rays entering the eye pupil at different points and a new colour effect. *Proceedings of the Royal Society of London. Series B, Biological Sciences*, 90-118.

[18] Enoch, J. M., & Stiles, W. S. (1961). The colour change of monochromatic light with retinal angle of incidence. *Journal of Modern Optics*, *8*(4), 329-358.

[19] Krantz, D. H. (1975). Color measurement and color theory: I. Representation theorem for Grassmann structures. *Journal of Mathematical Psychology*, *12*(3), 283-303.

[20] Alpern, M. (1986). The Stiles-Crawford effect of the second kind (SCII): a review. *Perception*, *15*(6), 785-799.

[21] Zhang, X., Ye, M., Bradley, A., & Thibos, L. (1999). Apodization by the Stiles-Crawford effect moderates the visual impact of retinal image defocus. *JOSA A*,*16*(4), 812-820.

[22] Marcos, S., Burns, S. A., & He, J. C. (1998). Model for cone directionality reflectometric measurements based on scattering. *JOSA A*, *15*(8), 2012-2022.

[23] Gorrand, J. M., & Delori, F. C. (1997). A model for assessment of cone directionality. *Journal of Modern Optics*, *44*(3), 473-491.

[24] DeHoog, E., & Schwiegerling, J. (2009). Fundus camera systems: a comparative analysis. *Applied optics*, *48*(2), 221-228.

[25] Colenbrander, A. (2009). Principles of Ophthalmology. *Duane's Ophthalmology. 15th ed. Philadelphia, Pa: Lippincott Williams & Wilkins*.

[26] Gullstrand, A. (1910). Neue methoden der reflexlosen ophthalmoskopie.*Berichte Deutsche Ophthalmologische Gesellschaft*, *36*.

[27] Pomerantzeff, O., Webb, R. H., & Delori, F. C. (1979). Image formation in fundus cameras. *Investigative ophthalmology & visual science*, *18*(6), 630-637.

[28] Saine, P. Focusing The Fundus Camera: A Clinical Approach. *Davis Duehr Eye Associates*

[29] Liang, J., Williams, D. R., & Miller, D. T. (1997). Supernormal vision and high-resolution retinal imaging through adaptive optics. *JOSA A*, *14*(11), 2884-2892.

[30] Roorda, A., & Williams, D. R. (2002). Optical fiber properties of individual human cones. *Journal of Vision*, *2*(5), 4.

[31] Vohnsen, B., & Rativa, D. (2011). Ultrasmall spot size scanning laser ophthalmoscopy. *Biomedical optics express*, *2*(6), 1597-1609.

[32] Gorrand, J. M., & Delori, F. (1995). A reflectometric technique for assessing photorecelptor alignment. *Vision Research*, *35*(7), 999-1010.

[33] Vohnsen, B. (2014). Directional sensitivity of the retina: A layered scattering model of outer-segment photoreceptor pigments. *Biomedical optics express*,*5*(5), 1569-1587.

[34] Atchison, D. A., Smith, G., & Smith, G. (2000). Optics of the human eye.

[35] Van Stryland, E., Williams, D., & Wolfe, W. (1996). *Handbook of optics (Vol. 2)*. M. Bass (Ed.). McGraw-Hill.

[36] Hecht, E. (2002). Optics. *Addison Wesley*.

[37] Sacek, V. Notes on amateur telescope optics, 2006.

[38] Roorda, A., & Williams, D. R. (1999). The arrangement of the three cone classes in the living human eye. *Nature*, *397*(6719), 520-522.

[39] Steinman, R. M., Haddad, G. M., Skavenski, A. A., & Wyman, D. (1973). Miniature eye movement. *Science*, *181*(4102), 810-819.

[40] Wu, J., Seregard, S., & Algvere, P. V. (2006). Photochemical damage of the retina. *Survey of ophthalmology*, *51*(5), 461-481.

[41] Andor sCMOS Brochure

[42] Andor sCMOS White Paper

[43] Vohnsen, B., Qaysi, S., Anjos, P., & Valente, D. (2015). Exploring Photoreceptor Directionality using Quadrant Pupil Detection. In: ARVO 2015 Annual Meeting; 2015 May 3-7; Denver, Colorado. Abstract nr 4080.

[44] Delori, F. C., Webb, R. H., & Sliney, D. H. (2007). Maximum permissible exposures for ocular safety (ANSI 2000), with emphasis on ophthalmic devices. *JOSA A*, *24*(5), 1250-1265.

[45] Andor Neo sCMOS Specifications

Appendices

A.1 Health and Safety

Table A.1 Maximum Permissible Radiant Power MPΦ (in watts) entering the natural or dilated pupil [44]

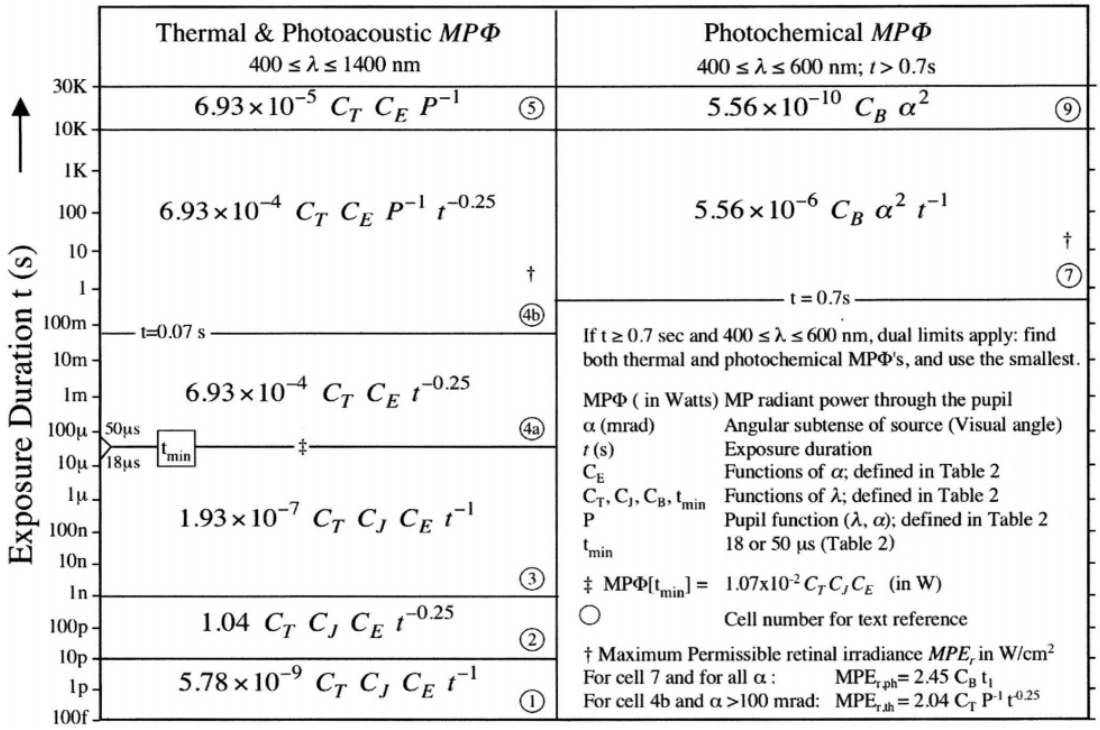

Table A.2 Parameters to be used in table A.1 [44]

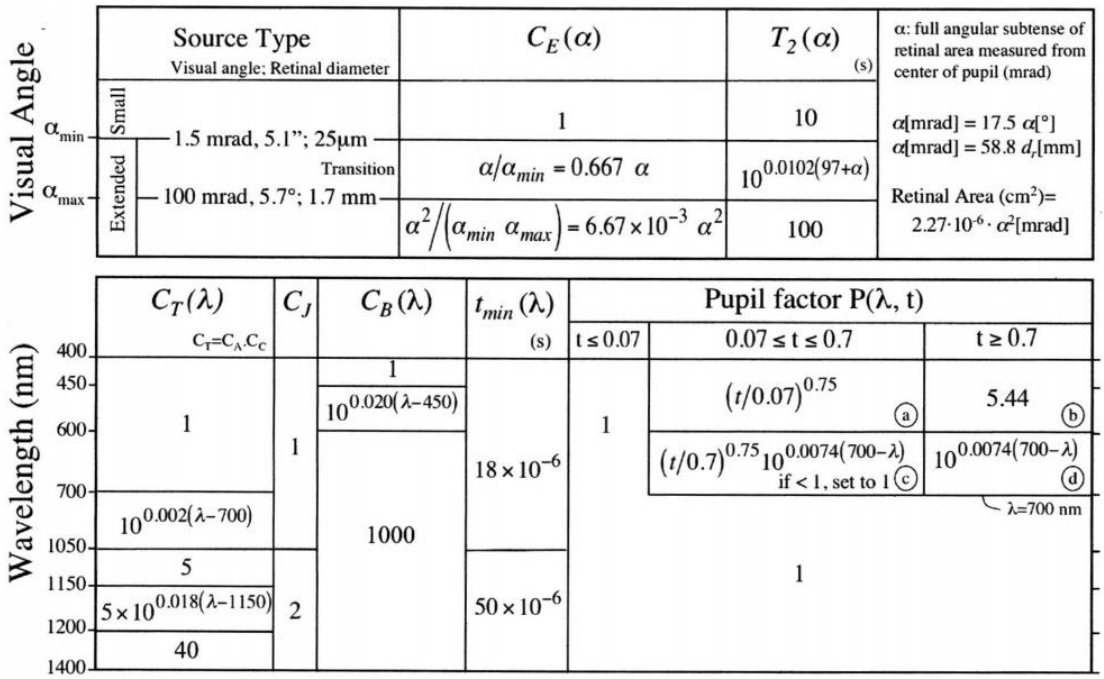

Thermal MPΦ calculation according to table A.1 and A.2:

$$MP\Phi_{thermal} = 6.93 \times 10^{-4}\ C_T\, C_E\, P^{-1}\, t^{-0.25}$$

$$\lambda = 650\ nm\ ;\ \alpha = 73.9\ mrad\ ;\ t = 30\ s$$

$$C_T = 1\ ;\ P = \ 10^{0.00743\ (700-\lambda)} = 2.34\ ;\ C_E = 0.667\ \alpha = 49.3$$

$$MP\Phi_{thermal} = 6.24\ mW$$

Photochemical MPΦ calculation according to table A.1 and A.2:

$$MP\Phi_{photochemical} = 5.56 \times 10^{-6}\ C_B\ \alpha^2\ t^{-1}$$

$$C_B = 1000\ \ ;\ \ \alpha = 73.9\ mrad\ \ ;\ t = 30\ s$$

$$MP\Phi_{photochemical} = 1.01\ W$$

Comparison between the maximum Φ used and the lowest value obtained for the maximum permissible:

$$\frac{30\ \mu W}{6240\ \mu W} \cong 0.005$$

As it can be seen, the maximum radiant power used in the experiments was well below the maximum permissible.

A radiant power of 100 µW was also used for periods of 1 second, for such a period of time the maximum permitted is even higher, hence, the radiant power used is still well below.

A.2 Sensor Specifications

Table A.3 Key specifications of the Andor Neo 5.5 sCMOS image sensor [45]

Key Specifications		
Sensor Type	Front Illuminated Scientific CMOS	
Active Pixels	2560 x 2160 (5.5 Megapixel)	
Sensor Size	16.6 x 14.0 mm (21.8 mm diagonal)	
Pixel readout rate (MHz)	560 (280 MHz x 2 sensor halves) 200 (100 MHz x 2 sensor halves)	
Read Noise (e-)	Rolling Shutter	Global Shutter
200 MHz	1	2.3
560 MHz	1.3	2.5
Minimum temperature air cooled	-30 °C	
Minimum temperature coolant	-40 °C	
Dark current, e-/pixel/sec		
@ -30°C	0.015	
@ -40°C	0.007	
Data range	12 bit & 16 bit	
Peak Quantum Efficiency	60%	
Readout modes	Rolling Shutter and Global (Snapshot) Shutter	
Internal memory buffer size	4 GB	
Maximum burst frame rates		
2560 x 2160 (full frame)	100 fps Rolling Shutter, 49 fps Global (Snapshot) Shutter	
128 x 128 ROI	1,639 fps Rolling Shutter, 716 fps Global (Snapshot) Shutter	
Pixel well depth (e-)	30,000	

A.3 System Development Photographs

Figure A.1 Photograph of the system with the telescope configuration

Figure A.2 Photographs of the system after the removal of the telescope, installation of the sensor and proper shielding. The light source (the tip of optical fibre) is completely shielded with black card and a soft plastic fabric.

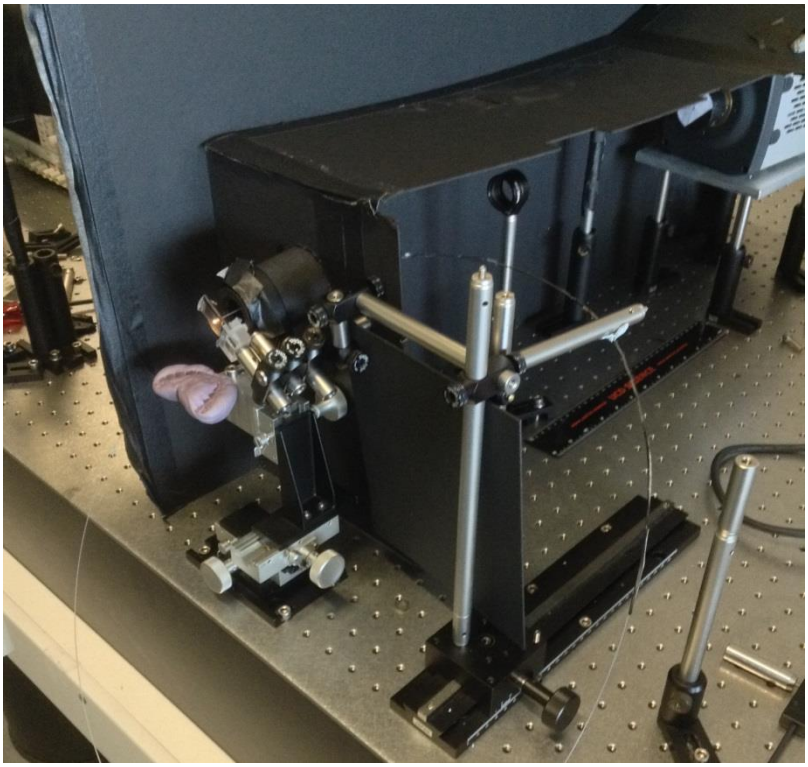

Figure A.3 Photograph of the experimental setup using the thin optical fibre for direct illumination of the eye

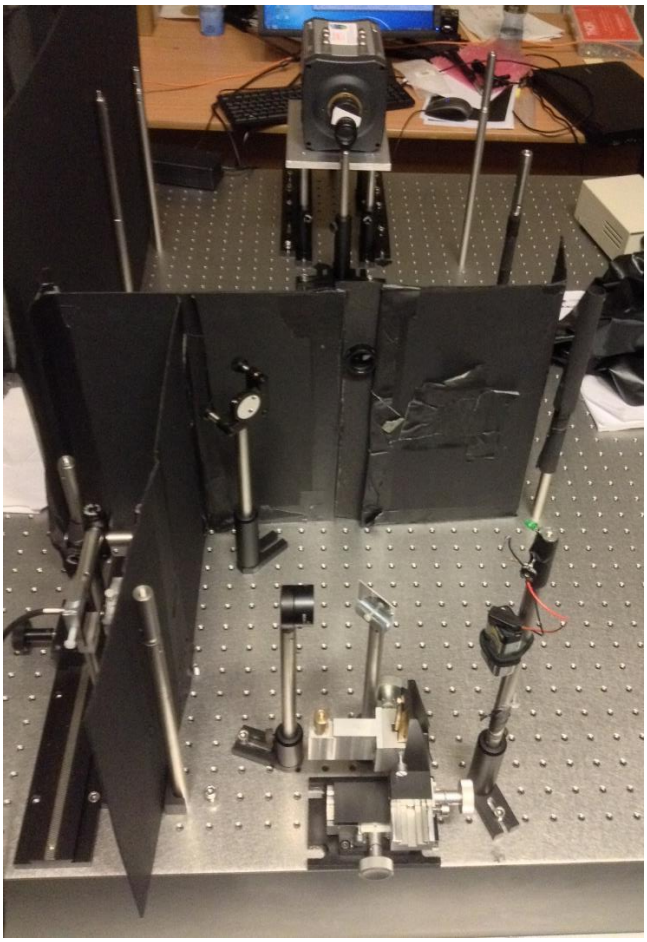

Figure A.4 Second attempt on the Maxwellian view method. Setup which produced the first images of cones at large eccentricities.

A.4 Photographs of the Final System

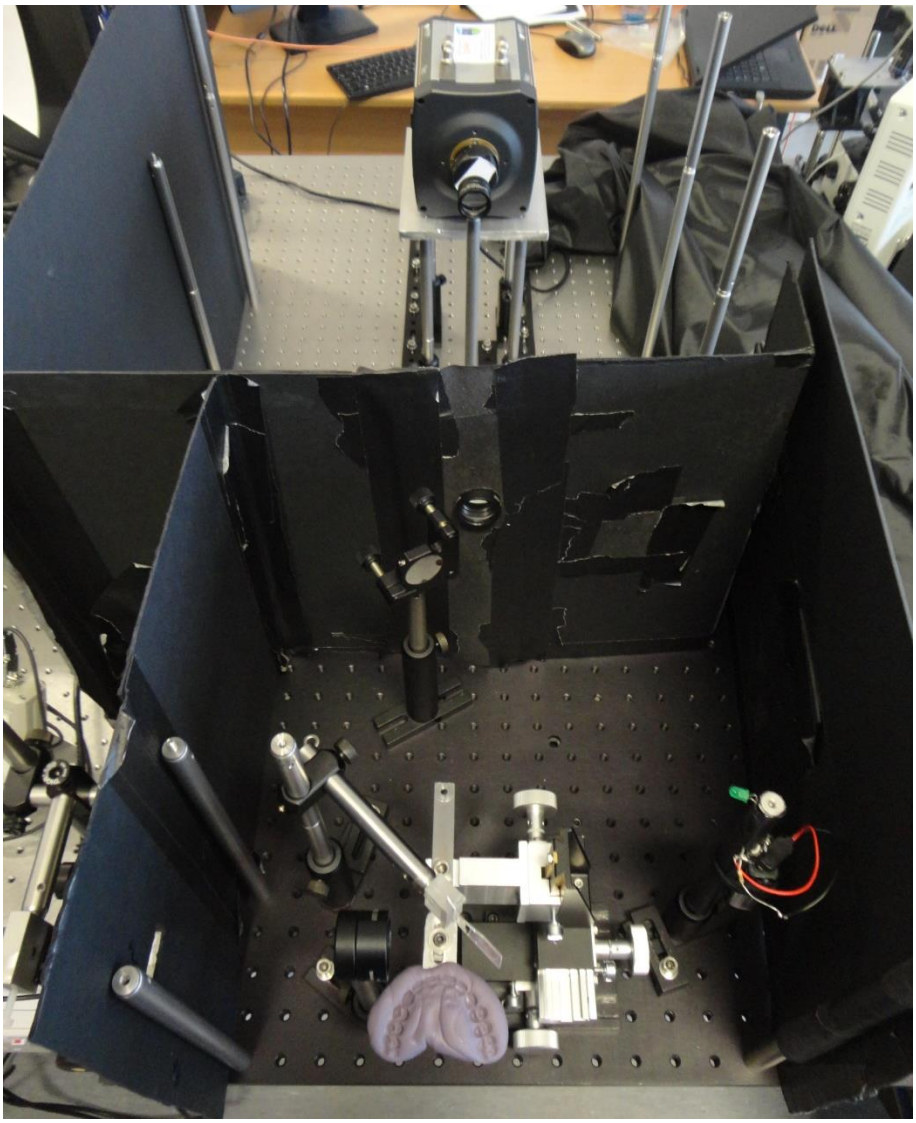

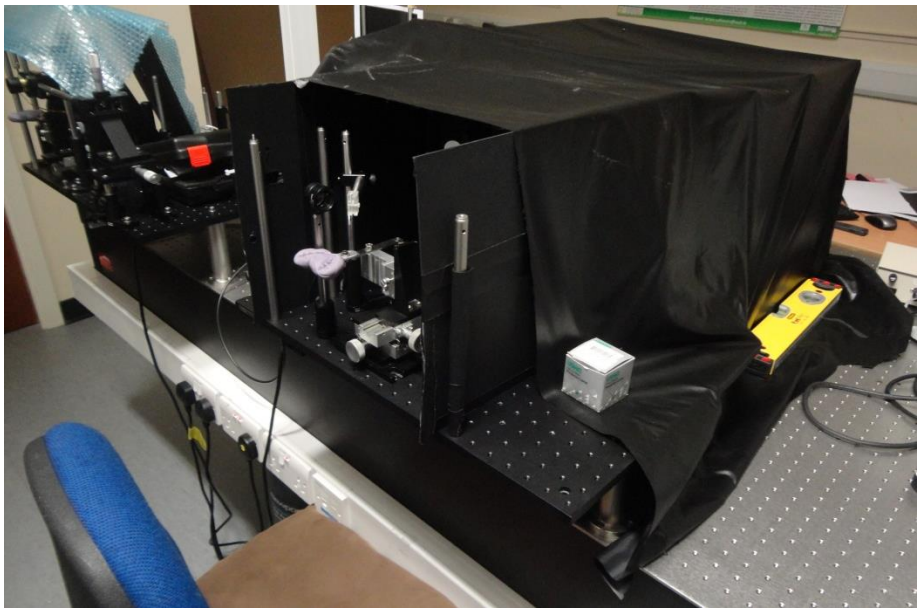

Figure A.5 to A.7 In order of appearance: final system uncovered; final system completely shielded; final system with main optical elements, no shielding or auxiliary elements such as metal rods or the LED are present.

A.5 Cone Mosaic and Capillary Images

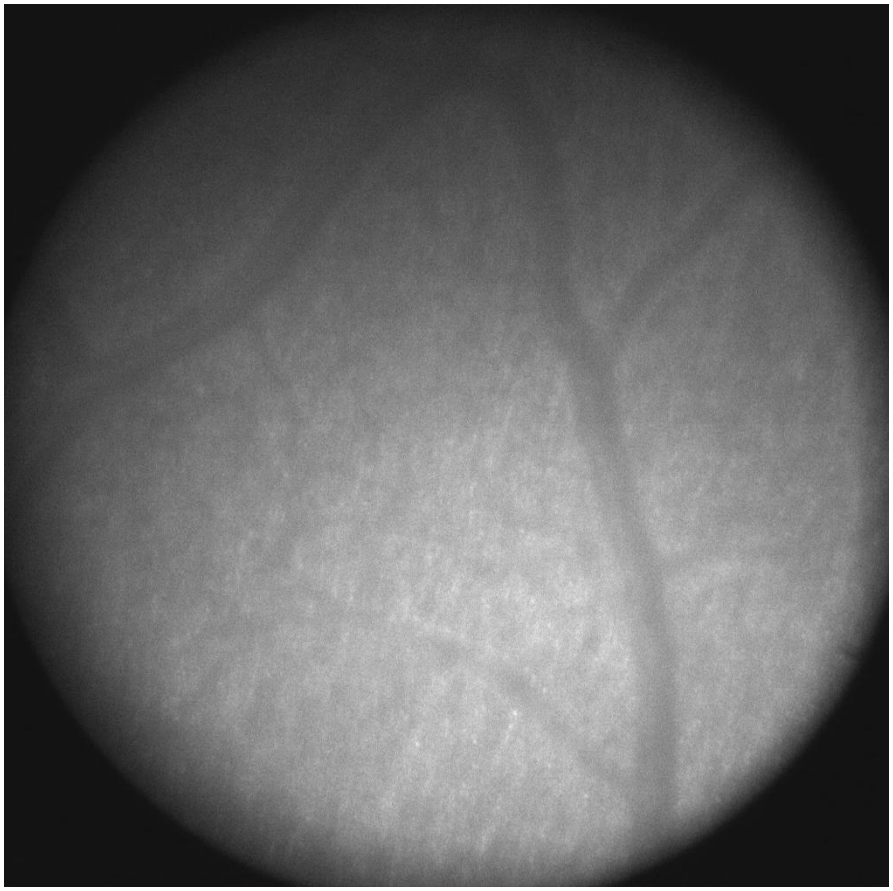

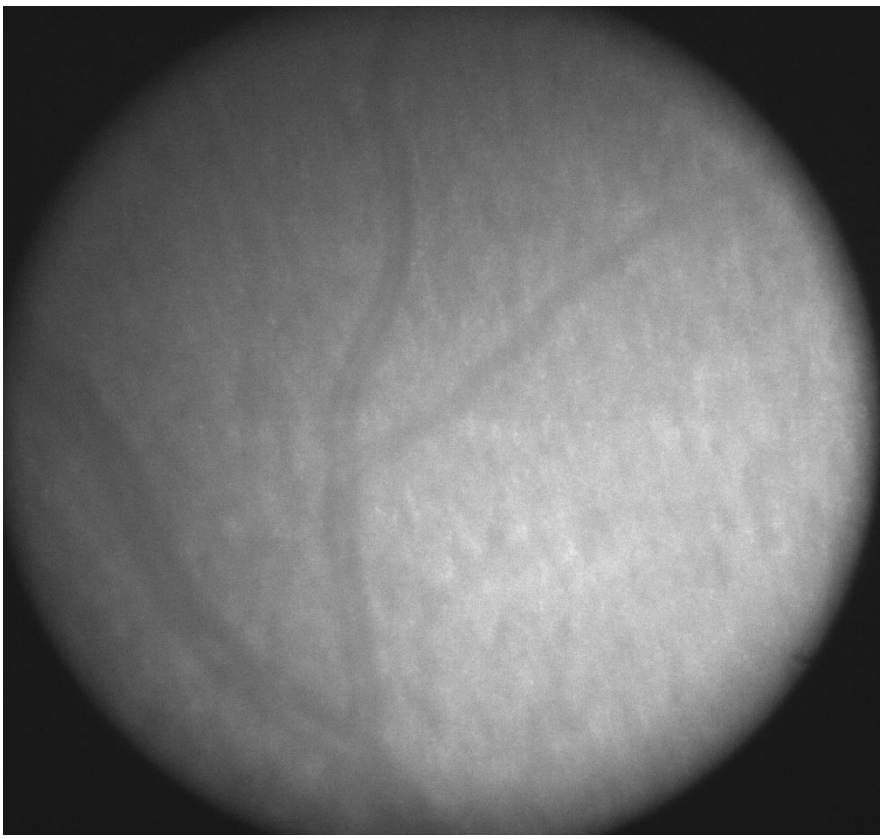

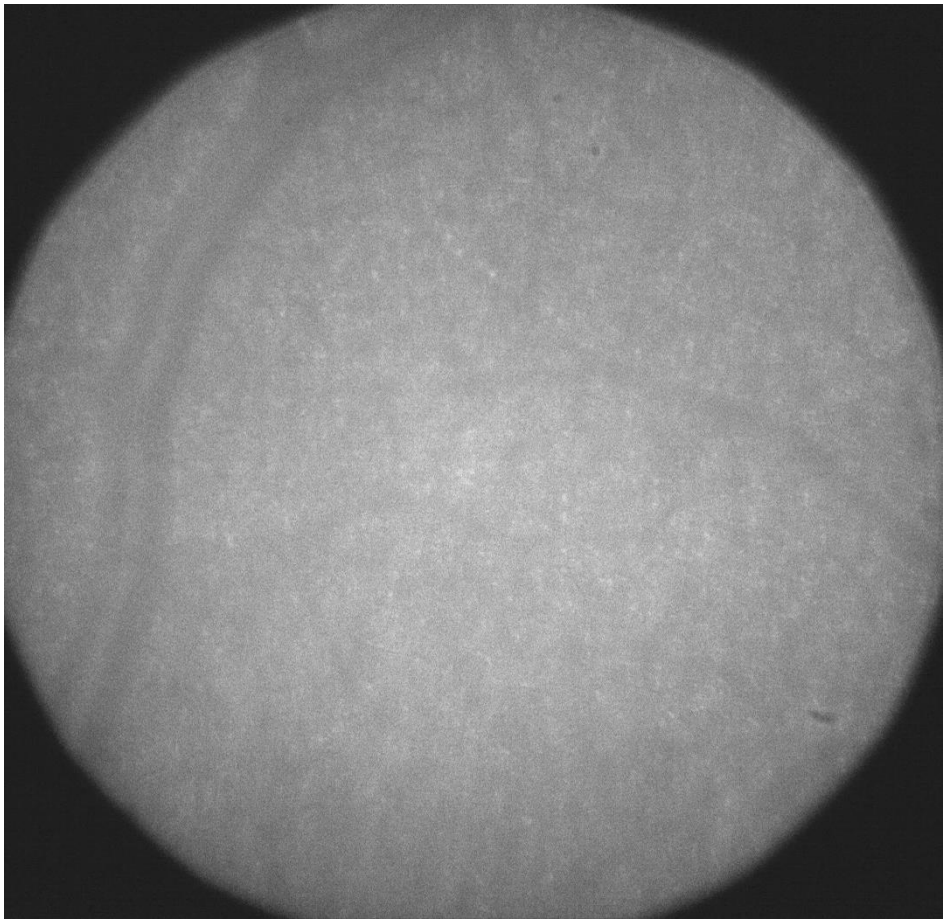

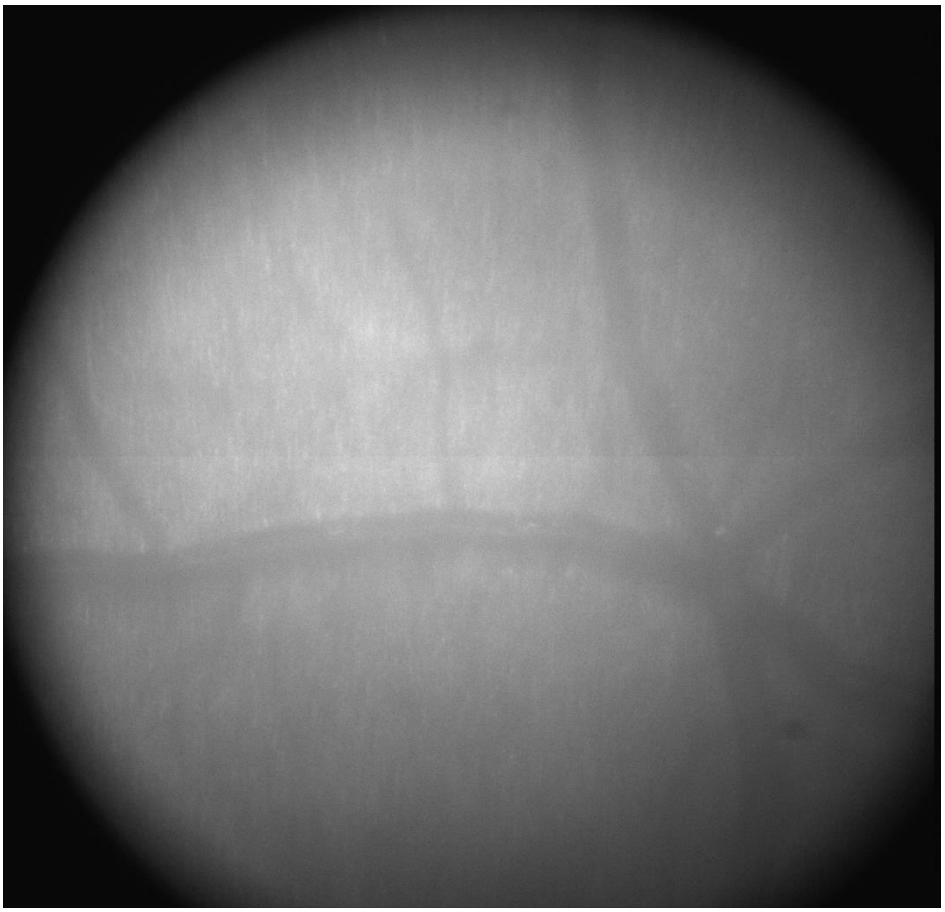

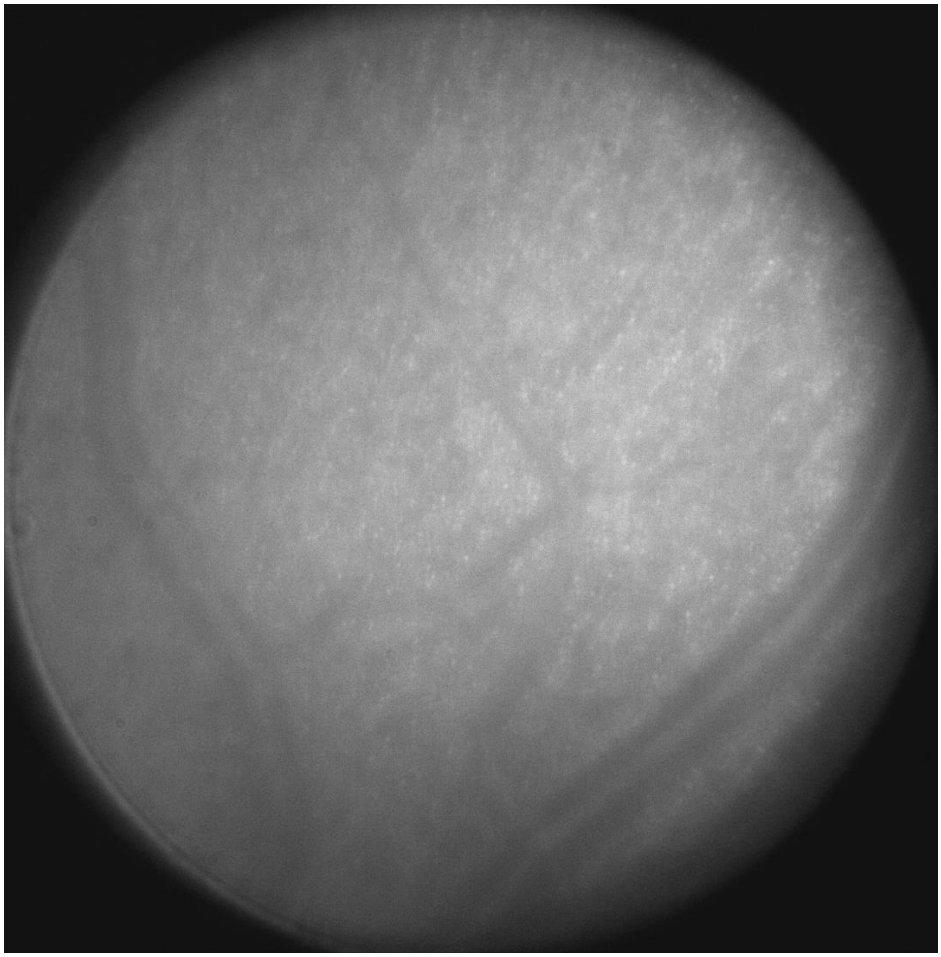

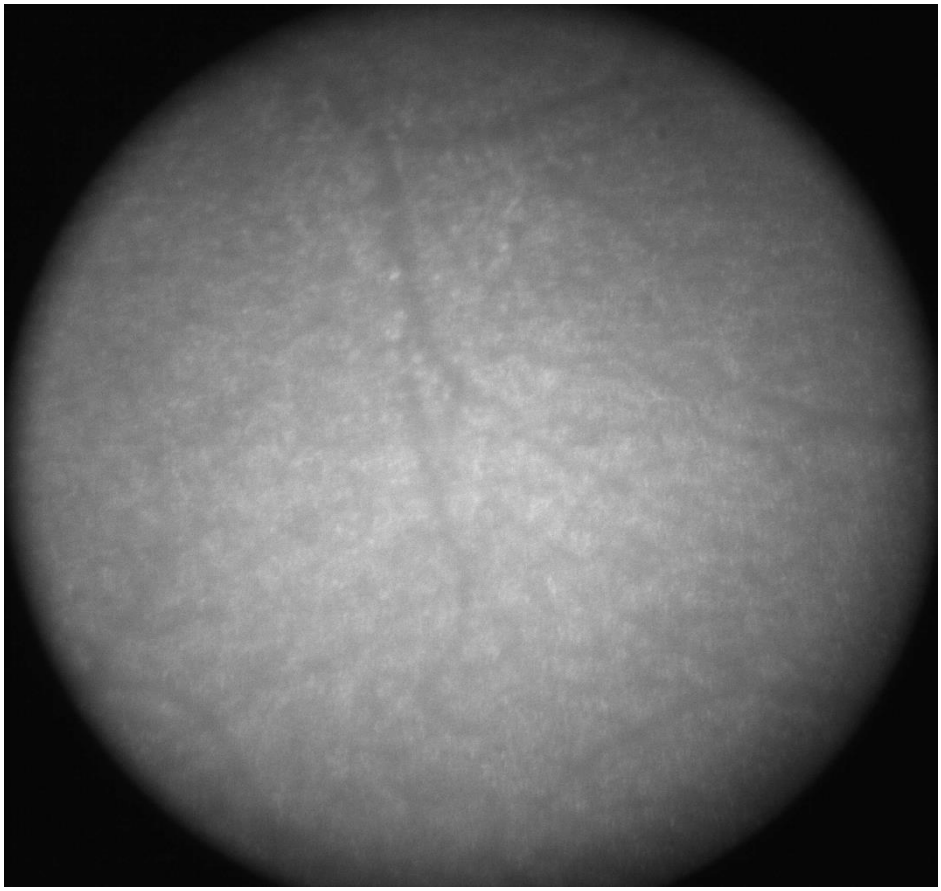

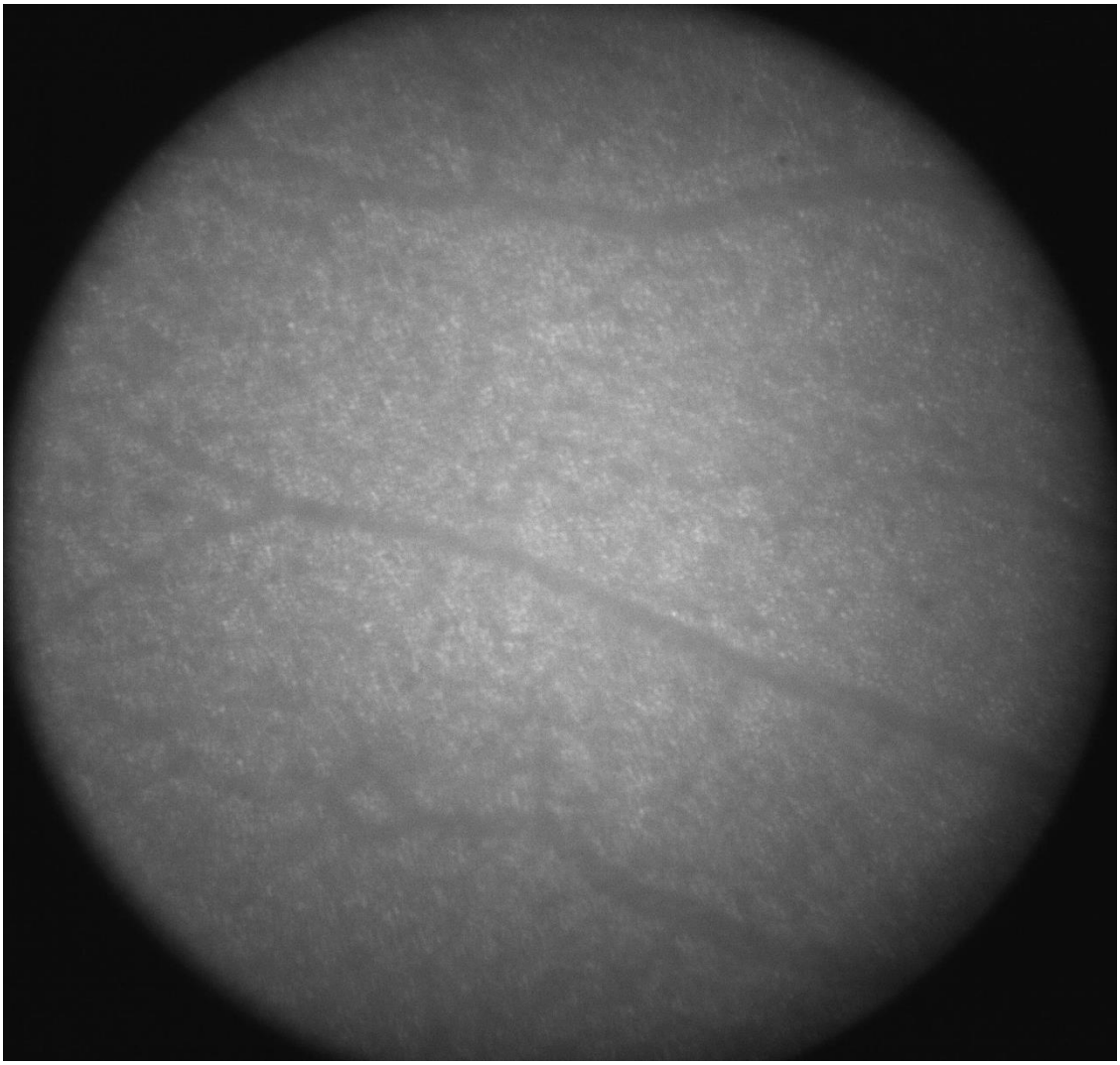

Figure A.8 to A.14 Parafoveal retinal images obtained with a magnification of 11.5 times. The last two images were obtained from the author's right eye while wearing myopic refraction correction.